High Resolution Multi-Axial Strain Measurement for Predicting Mechanical Response of Semi-Crystalline Polymeric Materials

E O AKHIGBE

2018

High Resolution Multi-Axial Strain Measurement for Predicting Mechanical Response of Semi-Crystalline Polymeric Materials

EROMOSELE ODIGIE AKHIGBE

A thesis submitted in partial fulfilment of the requirements of

Manchester Metropolitan University

for the degree of Master of Philosophy

Department of Engineering

Manchester Metropolitan University

2018

Abstract

Semi-crystalline polymeric materials such as High-Density Polyethylene (HDPE) are generally assumed to have a constant Poisson's ratio of 0.4. A study that was previously carried out on HDPE polymer by Bhabha in 2015 indicated that the Poisson's ratio may be non-uniform within the elastic region. This research establishes the variation in the Poisson's ratio of HDPE polymer below 1% strain, however, the Poisson's ratio stabilised as the strain increases within the elastic region. Poisson's ratio is a function of strain, both in the transverse and longitudinal direction of the material.

Strain is commonly measured using external transducers but can be limited by the difficulty in attaching strain gauge to the HDPE surface and can also alter the measured strain over the attached area if the stiffness of the material is significantly less than the stiffness of the strain gauge. Strain can also be measured using mechanically attached extensometers, which tend to indent soft materials thereby causing local stress within the area of contact. Due to these limitations, two non-contact methods were used in the research.

A non-contact optical technique known as Digital Image Correlation (DIC) was employed to investigate the strain and generate strain maps of the surface of HDPE and General-Purpose Polystyrene (GPPS) materials. The strain obtained was then used to calculate the Poisson's ratio for both materials.

The findings of the DIC technique was that the Poisson's ratio was non-uniform within the nominally elastic range of HDPE and GPPS polymer. The DIC technique is a full-field technique and the results showed non-uniformity in Poisson's ratio at 1% strain, however, as the strain increases, the Poisson's ratio stabilises to a constant value.

From the DIC results obtained, there is no direct comparison between the behaviour of HDPE and GPPS on the surface. The hypothesis is that the non-uniformity in strain and hence the Poisson's ratio obtained from the DIC techniques could be related to local relief of stresses occurs when crazes form, which could lead to the modulations in lateral and longitudinal strain in the case of GPPS material. Whilst in HDPE, there are localised movements of the crystal lamellae. Also, a likely explanation could be that at the strain range investigated could only cause significant deformation in the amorphous regions whilst the crystalline regions are unaffected.

A further investigation on the internal composition will be required to further understand the results obtained on the surface of the specimens.

Acknowledgements

First and foremost, I would like to thank God Almighty for His grace and guardians through this research, without Him I would not have successfully completed this research.

To my Director of Studies, Dr. Howard Taylor and my supervisors, Dr. Weizhuo Wang and Dr. Christopher Liauw thank you for your advice, time and wide range of experience offered to me throughout this research.

I would like to thank Digital Horizon Co. Ltd for financially sponsoring me throughout this research, I am indeed grateful and favoured.

Finally, thank you to my parents Surv. Akhigbe Irenen JP and Mrs Philomena Irenen for the love and moral support you have shown me over the years. To my lovely family, Jeffery Akhigbe, Emily Akhigbe and especially my wife Mrs Rosemary Akhigbe LLM & LPC, thank you for standing by me through this research journey. I love you all and I am very grateful to have you in my life.

Thank you.

Table of Contents

List of Tables

List of figures

Abbreviations

DIC	Digital Image Correlation
DSC	Differential Scanning Calorimetry
FEA	Finite Element Analysis
GPPS	General Purpose Polystyrene
HDPE	High Density Polyethylene
JPEG	Joint Photographic Expert Group
TIF	Tagged Image Format
USB	Universal Serial Bus
υ	Poisson's Ratio

Chapter 1 Introduction

This chapter comprises of the background of this research, the aims and the objectives of this project.

1.1 Background of the Research

Polymers are highly used in various industries such as aerospace engineering. For instance: the Airbus A350 XWB was built with 52% carbon-fibre reinforced polymer (CFRP)(Airbus Group, 2006). In other industries such as automotive and civil engineering, strength-to-weight ratio is paramount. It is therefore necessary to know the mechanical properties and response of the material. Material response simply means how the material reacts to the load applied (Yan *et al.*, 2006). Polymers have complex non-linear behaviour depending on the strain rate, temperature, structural parameters such as degree of crystallinity, molecular weight and others (Ayoub *et al.*, 2010).

Recent investigations conducted by Bhabha in 2015 on unfilled and filled High Density Polyethylene (HDPE), indicated that the Poisson's ratio (υ) value was indeterminate within the elastic region but stabilised at higher levels of strain that were close to the yield point as shown in Figure 1. Apart from the non-uniformity in Poisson's ratio values obtained, several values up to 0.5% strain were above the expected range of 0.4 and various negative values were also recorded. As a result, it was decided to investigate further the Poisson's ratio versus tensile strain of unfilled HDPE.

HDPE is semi-crystalline in molecular structure and is one of the most popular polymers and is widely used in a wide range of applications due to its properties (Şirin *et al.*, 2013). This is the reason why it was selected as the research material.

In order to effectively analyse the material response of structures manufactured from HDPE, accurate information about the mechanical properties of HDPE is required (Khalajmasoumi *et al.*, 2012). The information required for Finite Element Analysis (FEA) varies depending on the type of analysis to be carried out. A non-linear analysis for example requires the Poisson's ratio value and stress-strain data of the specific material to be analysed.

Poisson's ratio value is defined as the ratio of lateral strain to the longitudinal strain under extension or compression (Tschoegl *et al.*, 2002). Generally, with polymers, the Poisson's ratio value typically varies from -0.5 to 0.5 depending on the type of material (Brown, 1999; Khalajmasoumi *et al.*, 2012). Most engineering materials have a Poisson's ratio varying from 0.33 to 0.46. The Poisson's ratio for HDPE was measured to be 0.45 (Beijer and Spoormaker, 2002). Other materials with their typical Poisson's ratio values are shown in Table 1.

Table 1: Materials with their Poisson's ratio values (Callister and David, 2010).

Aluminium	0.33
Steel	0.30
Copper	0.34
Rubber	0.48 - ~0.5

As stated earlier, Poisson's ratio is derived from the strain obtained by testing the material and the strain is defined as the change in length divided by the original length. Strain measurement was commonly determined by sticking foil strain gauges to the material or

using extensometers, which are subject to limitations (Lin *et al.*, 2014). Due to advancement in technology, the use of contact techniques such as foil gauges and extensometer have been replaced by non-contact techniques (Hoult *et al.*, 2013). As time unfolds, the application of non-contact techniques is on the rise and the effectiveness has been proven beyond any doubt over several years as recorded by Sutton (Schreier *et al.*, 2009). As such, two non-contact techniques (twin microscope and digital image correlation) were used to track the movement of the markers or random pattern on the HDPE specimen surface in order to obtain displacements, which were then used to obtain strain and ultimately Poisson's ratio. The initial part of this study is focused on obtaining the Poisson's ratio (υ) using the twin microscope technique.

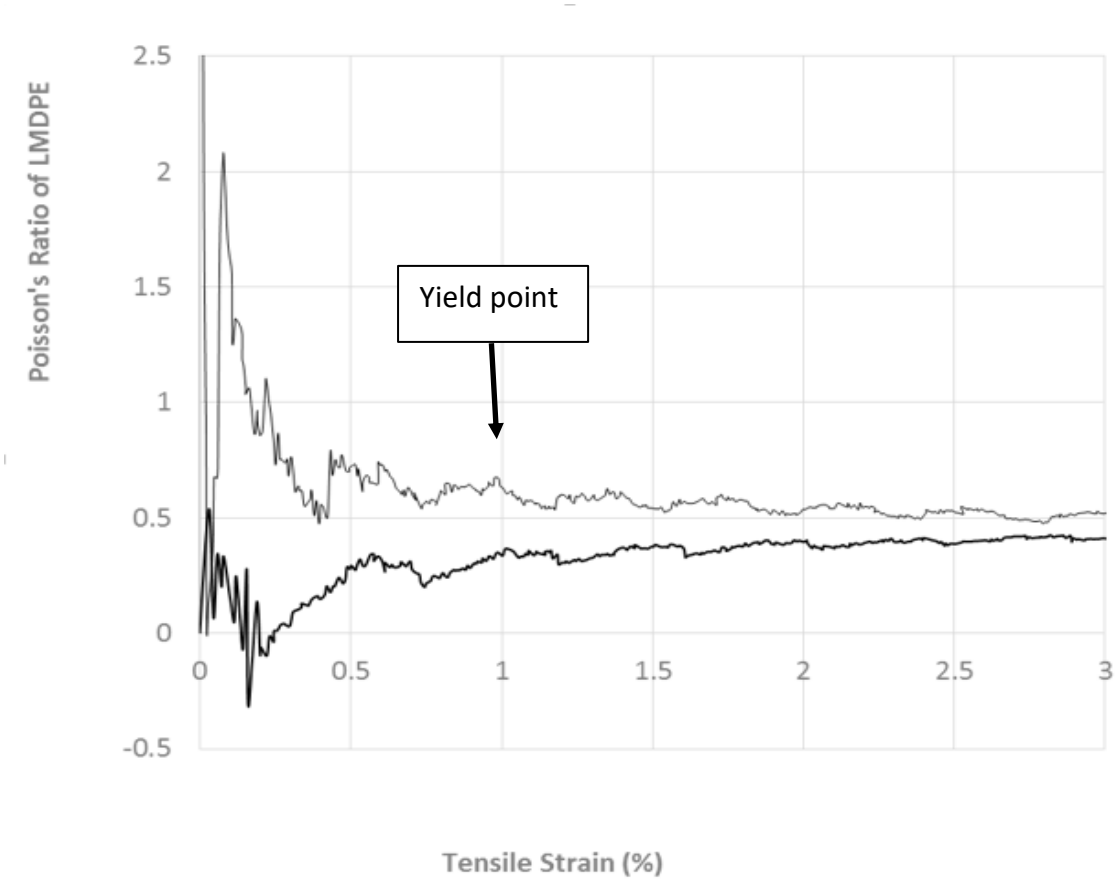

Figure 1: Poisson ratio against tensile strain for two HDPE specimens (Bhabha, 2015).

The Digital Image Correlation (DIC) technique analyses speckle pattern (a random array of dots) to obtain the displacement and strain, which can then be used to calculate Poisson's ratio. The results of the DIC technique will be used to obtain more detailed Poisson's ratio results over a larger area.

1.2 Aim and Objectives

1.2.1 Aim of the Research

To investigate the variation of Poisson's ratio in HDPE and GPPS as a function of tensile strain below the yielding point.

1.2.2 Objectives of the Research

a) To examine previous work done to obtain strain and Poisson's ratio in HDPE polymer.
b) To monitor the displacement of a defined area on the surface of stressed HDPE specimens.
c) To investigate the strain distribution within a defined area in both longitudinal and transversal direction of HDPE using DIC.
d) To compare the strain map of semi-crystalline (HDPE) and amorphous (GPPS) material.
e) To investigate the variation in Poisson's ratio within the elastic limit of HDPE and GPPS using DIC.

Chapter 2 Literature review

In this chapter, a background study of polymeric materials, strain measurement techniques and Poisson's ratio will be discussed.

2.1 Polymeric Materials

We are constantly surrounded by different kind of materials from the cloths we wear, sunglasses, shoes, mobile phones, houses and the cars we drive as we live our lives daily. There are different types of material such as metals, plastic, wood and glass among others. Materials such as steel have been replaced by unfilled and filled polymeric materials in many areas such as storage and transportation of gas, car chassis, airplane wings and fuselage, due to the material's long-term durability against degradation and its low cost (Kiass *et al.*, 2005; Frank *et al.*, 2009).

Polymer is a large molecular chain comprised of many smaller structural units called monomers. The atoms within the polymer molecules are covalently bonded together in any conceivable pattern (Cowie and Arrighi, 2007). As the application of polymeric materials increases, it is fundamental to understand its response under different loading conditions (Velosa *et al.*, 2008; Ayoub *et al.*, 2010).

Some polymers consist of amorphous regions which are formed by disorder in the molecular chain structure of the material (Callister and David, 2010). Amorphous polymers such as General-Purpose Polystyrene (GPPS) are defined as materials that do not exhibit any crystalline structures in X-Ray Diffraction (XRD) (Vecchioc *et al.,* 2005). About their melting temperature, amorphous polymers have intertwined chains. Elastic and plastic deformation can easily occur when load is applied, and the elastic deformation may be

recovered when the load is removed, however, the shape would have been permanently altered. In lower temperature, the amorphous polymer becomes stiffer and stronger as the viscosity reduces (Askeland, 1990). Amorphous material may also indicate the inability to crystallise, either due to its constitution or under specific circumstances such as when subjected to fast cooling conditions (Allegra *et al.*, 1989).

General purpose polystyrene (GPPS) is formed by joining styrene monomer molecules into a long polymer chains (Massey and Massey, 2005). GPPS is transparent, hard, brittle and resistant to heat. Polystyrene is an amorphous material and it exists in a glass form provided the temperature is below 100^{o}c, therefore, GPPS is used in optical, food and drink packaging, automotive, medical and electronic applications (Kricheldorf et al., 2004).

In other polymers, crystalline regions (molecular chains are closely aligned in a pattern) of a lamellar structure at the submicron level is surrounded by amorphous regions; this known as semi-crystalline polymer (Jar, 2015). HDPE is an example of semi-crystalline polymer as it is comprised of crystalline regions surrounded by amorphous regions. The crystalline regions have relatively high stiffness compared to the amorphous regions, which have relatively low stiffness. Polymers have a wide range of mechanical, physical and chemical properties. When HDPE is under a uniaxial load, the amorphous region first undergoes deformation due to its relatively low stiffness and then the surrounding crystalline region deforms gradually. As a result of the molecular structure, HDPE is not truly elastic but visco-elastic, which implies that there is always some inelastic deformation occurring within the elastic region of the material (Ayoub *et al.*, 2010).

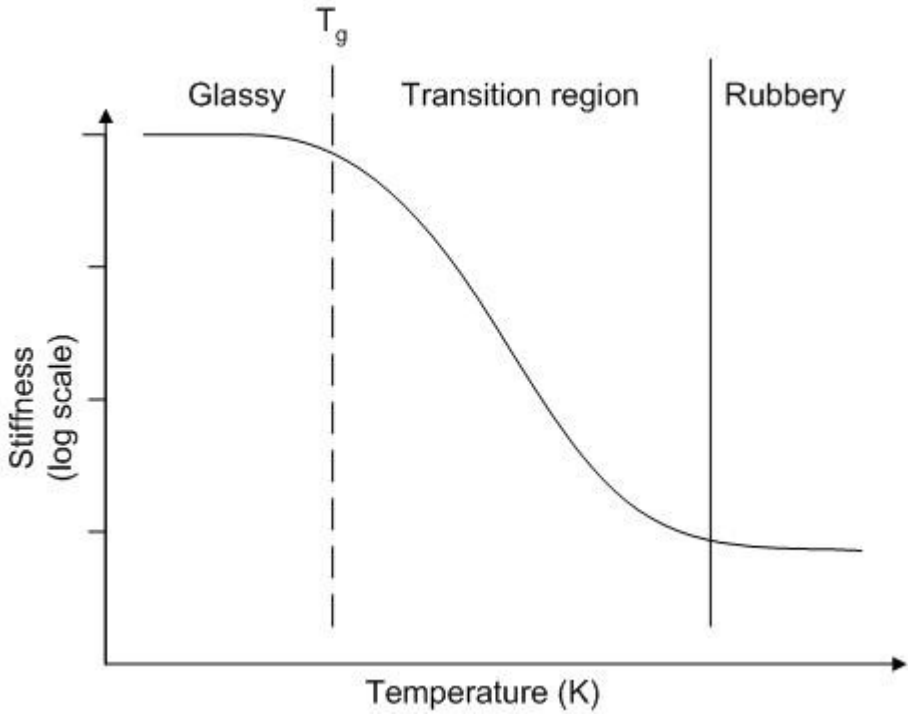

Figure 2: The Phase of polymer behaviour (Tangram Technology Ltd, 2013).

Most polymers partially crystalize when cooled below their glass to rubber transition temperature. Figure 2 shows a graph of stiffness and temperature for polymers, indicating the glass transition temperature (Tg). Also, from figure 2, it is shown that Young modulus (measure of stiffness) of polymeric materials is higher at low temperature.

Polymeric materials can be categorized by their molecular structure (arrangement of their molecular chains). The molecular structure of polymers could be linear, branched, crosslinked and network. The chains in a linear structured polymer could be very long and primarily possess linear chains (lack of branches). As a result, they tend to pack closely together such as high-density polyethylene (HDPE). Crystallization is easily accomplished in linear polymer because of fewer branched chain to prevent chain alignment. Polymer with branched chain structure have side chains connected to the main chain are called branched polymer. The branched chains reduce the chain packing efficiency thereby

lowering the density of the polymer such as low-density polyethylene (LDPE) material. In the case of crosslinked polymers, adjacent linear chains are connected by atoms or molecules by covalent bonds such as rubber. In networked polymers, the monomers form multiple active covalent bonds creating a three-dimensional network such as polyurethanes and phenol-formaldehyde (Callister and David, 2010).

The amorphous region possessing viscoelastic behaviour when in rubbery state. Crystalline region is formed by folding of long polymer molecules and they mainly deform by crystallographic slip as shown in Figure 3 (Nikolov *et al.*, 2002).

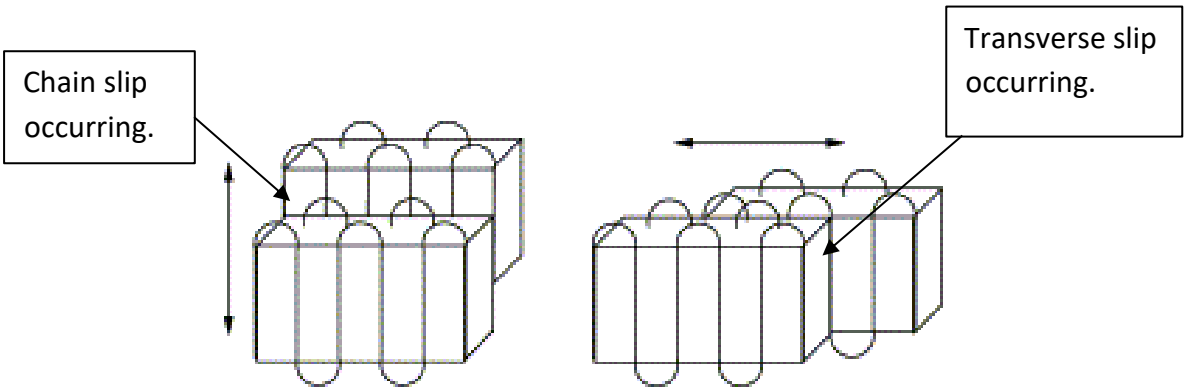

Figure 3: Deformation of crystalline lamellae (Nikolov *et al.*, 2002).

In summary, for HDPE, the amorphous regions surround the crystalline regions and due to their relatively low stiffness, the amorphous regions are expected to deform more than the crystalline regions, which may then lead to variation in strain distribution across the material.

In the next section of the literature review, strain measurement techniques will be discussed.

2.2 Strain Measurement

In the previous section, the structure of semi-crystalline polymeric material was discussed and how the material structure influences deformation when subjected to loading was reviewed. This section will focus on the definition of strain and how it can be effectively measured.

Strain is a measure of the relative displacement of the constituents without the material undergoing rigid body motion (McClung *et al.*, 2011). Strain can be measured using contact and non-contact methods. Contact method such as strain gauges and extensometers are popularly used to measure the surface strain of a structure (Esmaeili *et al.*, 2012). Strain gauges consist of a metallic foil pattern supported by an insulating flexible backing and is glued onto the surface of the specimen and clip-on extensometers consist of four knife edges, which are used to hook the specimen. Strain gauges only provide an average strain over the area covered by the gauge. In order to measure strain field of a surface, numerous foil strain gauges are required, and these foil strain gauges are then wired individually thereby making it physically difficult to map strain over small areas. Other limitations of the foil strain gauges are that they need to be bonded to the structure, which can impact the strain measurement if the stiffness of the material is not significantly greater than the stiffness of the strain gauge and bond instability may occur over long-term monitoring (Hoult *et al.*, 2013). In addition, clip-on extensometers tend to cause indentations in the material resulting in local stress within that area, when used on a soft polymeric material (Jerabek *et al.*, 2010).

Similar conclusions were drawn from literature that the limitations of both contact strain measuring methods can be circumvented by the use of non-contact techniques (McClung

et al., 2011). Non-contact techniques such as laser extensometer and optical or DIC techniques can be used to measure the surface strain of a specimen. Advantages of using non-contact techniques such as the DIC techniques are as follows: (a) full-field monitoring, (b) cost effective and (c) can be used for small and soft materials without having contact issues (Hoult *et al.*, 2013).

In conclusion, it is generally agreed that to adequately measure the strain on the surface of softer materials, non-contact techniques are recommended due to the advantages as listed earlier.

2.2.1 Digital Image Correlation

This section will be focused on a brief history of DIC technique and how DIC was applied. Peters and Ranson (1982) in one of the earliest papers proposed the use of computer-based image acquisition and deformation measurement in materials (Peters and Ranson, 1982). In 1983, the numerical algorithm was developed and experiments were performed by Sutton *et al* (Sutton *et al.*, 1983). The use of DIC technique has grown in different areas such as fracture mechanics, nanotechnology and fluid mechanics among others (Schreier *et al.*, 2009).

Numerical models are usually validated by conducting identical experiments and then comparing the results such as maximum stress or strain obtained from the numerical analysis with results from the experiment. In the experiments, strain gauges are positioned only in those areas where the stress is maximum, as indicated in the numerical model, thereby ignoring other potential areas (Wang *et al.*, 2011).

DIC technique is a full-field and non-contact strain measurement technique, unlike strain gauges and clip-on extensometers that measure a single strain value over the area

covered. DIC technique compares random pattern on deformed images with random pattern on an undeformed or reference image in order to determine the displacement and DIC technique has been proven to accurately measure strain in various applications where contact methods are not easily conducted (Hoult *et al.*, 2013).

One of the advantages of DIC is that plots of the strain distribution in longitudinal and transverse directions can be obtained from a single test and in turn Poisson's ratio can be calculated (Jerabek *et al.*, 2010). The DIC technique also has some limitations such as the specimen needs to be well lit and there must be no vibrations from the test equipment, surroundings and the camera. Also, the random pattern needs to adhere properly with the surface of the HDPE specimen being tested. HDPE material generally has poor wettability and adhesion properties which causes problems in numerous applications such as packaging and automotive industries where surfaces require coating and printing. Due to the difficulty in printing and coating on the surfaces of HDPE components, several methods have been developed to improve the adhesion attributes such as plasma, laser, corona and flame treatment where flame treatment is one of the methods widely used for surface activation of polymers (Farris *et al.*, 2010a). The rationale for choosing flame treatment was that the equipment required to carry out the test was readily available in the laboratory and the process was fast, easy to implement and effective.

Flame treatment, when used in surface activation breaks the C-H links between the molecules along the polymer surface due the temperature produced in the combustion process and adds oxygen-based groups within the broken links leading to new hydrophilic sites for interaction with the coating or printing element (Farris *et al.*, 2010; Tuominen et al., 2013). Flame treatment can be used to improve surface adhesion of thin component

profile made of polymer where the affected thickness is 5-10nm. The more oxygen-based groups on the surface of the material, the better adhesion results. Farris et al (2010) concluded that flame treatment is a powerful technique for enhancing the surface attributes of plastic materials mostly those with inherent hydrophobicity, however, for industrial use, more research is needed in the combustion phenomena and the initial settings of the parameters affecting the overall flame treating process compared to corona.

Figure 4 shows a thin square plate of steel with a circular hole in the centre subjected to tensile load. DIC technique was used to obtain strain maps at different loads (6.4kN, 12.9kN, 16.1kN, and 17.5kN). The results show high strain concentration around the hole. Similarly, DIC technique will be used to obtain strain map plots of HDPE specimen at different load intervals.

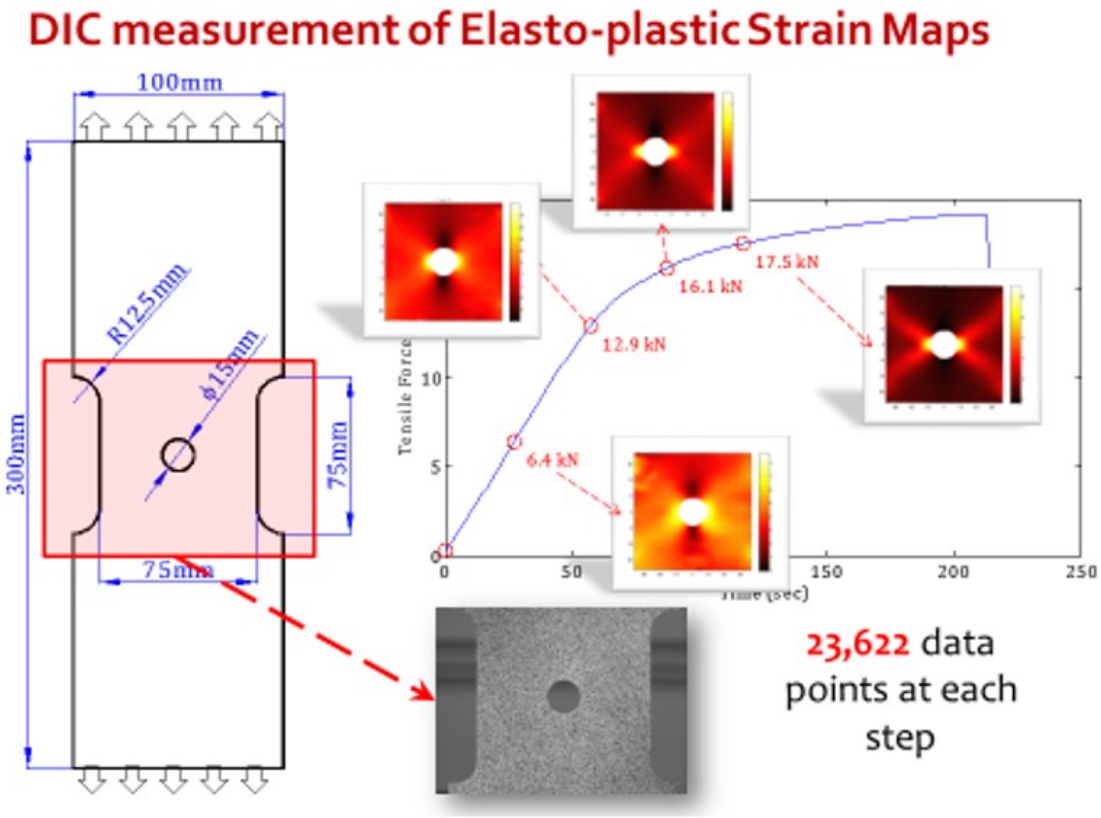

Figure 4: Strain maps at different load position using DIC (Wang *et al.*, 2011).

2.3 Background of Poisson's Ratio

This section will focus on the history, importance and how to obtain Poisson's ratio.

Poisson's ratio (υ) is defined as the ratio of lateral strain to axial strain in an axially loaded linear elastic solid (Bonfiglio and Pompoli, 2017). Poisson's ratio is a material property that governs the magnitude of transverse deformation when tensile or compressive stress is applied longitudinally (Lakes, 1987). Poisson's ratio of a material is positive if the material contracts in the transverse direction when tensile force is applied at the longitudinal direction. Poisson's ratio is negative (such as auxetic materials) if the material expands in the transverse direction when compressed force is applied in the longitudinal direction.

The range for Poisson's ratio for isotropic elastic materials is between -1.0 to +0.5 (Mott and Roland, 2009). As the Poisson's ratio value approaches 0.5, as found in rubber, the material is referred to as an incompressible material. When the Poisson's ratio value approaches -1.0, the bulk modulus is much less than the shear modulus and the material is said to be a highly compressible material. Most steels and rigid polymer exhibit Poisson's ratio value of about 0.3. When the Poisson's ratio value of a material approaches 0, it shows little change in the transverse direction such as corks. When materials exhibit negative Poisson's ratio value, when subjected to tensile strain in the longitudinal direction such as sponge, the material is referred to as auxetic material (Choi and Lakes, 1992). Poisson's ratio is measured at relative small deformation, where the mechanical response can be approximated as linear (Sanborn and Song, 2019).

Poisson's ratio is important because many mechanical behaviours of a material are related to its Poisson's ratio. Obtaining the Poisson's ratio also helps to identify which material is best suited for a certain application such as the cork of a wine bottle. The cork should be easily inserted and removed from the bottle, however, at the same time, it should be able to withstand the pressure from within the bottle. A material with υ of 0.5 cannot be used for this purpose because the material will expand when compressed into the neck of the bottle. Therefore, a material with near zero value of υ will be ideal in this application. Other applications for different materials are sponges, shock-absorbing materials, air filter and fasteners.

Chapter 3 Methodology of DIC technique.

This chapter describes the injection moulding conditions in which the test specimens were produced, how the DIC data was obtained and how the data was processed to produce results for HDPE material. This methodology was repeated for GPPS specimens.

The test specimens were injection moulded using the Battenfeld BA 230CD PLUS reciprocating screw injection moulding machine, set to the following conditions:

Hydraulic line pressure for HDPE	70 Bar
Hydraulic line pressure for GPPS	95 Bar
Hold pressure for HDPE	30 Bar
Hold pressure for GPPS	40 Bar
Injection time for HDPE and GPPS	11 Seconds
Cooling time for HDPE and GPPS	20 Seconds
Barrel temperature for HDPE and GPPS (at all zones)	200^{o}C

The Battenfeld BA 230CD PLUS reciprocating screw injection moulding machine was fitted with a tensile and impact test mould which had fan gates at the end of the impressions. Table 5 in Appendix A contains the materials and used. The test specimens were made to standard (ISO 527).

3.1 Overview of DIC technique

DIC technique is a non-contact optical method used to obtain full-field displacement and strain over a selected area. DIC technique involves generating random speckle patterns on the surface of the specimens to be tested, by using a black paint. The images were then captured with a camera before and after deformation.

The images captured were converted to grayscale format and imported to a Matlab algorithm for further processing. The images were arranged in the order they were captured and saved in that order. An array of control points was superimposed over the

user defined area of the first image. Each control point is surrounded by an area called subset. The subsets of the reference image are matched with similar subsets in the deformed image by identifying the speckle pattern within the subsets (this process is known as tracking).

The difference between the reference position of the subset in the reference image and the new position of the subsets in subsequent images results in displacement. The displacement obtained was then interpolated to produce strain. The displacement and strain were calculated over the user defined region, thereby producing a displacement and strain map over the region. The displacement and strain results can then be resented in various forms such as vector and contour plots. Poisson's ratio was then calculated from the both longitudinal and transverse strain.

The steps employed in the DIC technique such as generating speckle pattern on the specimens among others will be discussed in subsequent sections of this chapter.

3.2 Speckle pattern

In the previous section, an overview of the DIC technique was described and generating the speckle pattern was noted as one of the processes to be carried out in the DIC technique.

A speckle pattern is a random pattern generated to produce different grey scale values on the surface of the specimen. Speckle patterns can be generated by spraying paint or can be derived from the natural texture of the specimen surface (Hua *et al.*, 2011).

The success of DIC technique depends on the speckle pattern deforming simultaneously with the specimen, lack of vibrations within the experiment or surroundings. DIC

technique also depends on the quality of the speckle pattern used, therefore, it is important to produce good quality speckle pattern.

Random speckle patterns were initially generated by flicking a toothbrush dipped in black paint so as to project the paint on the surface of HDPE specimens. Figure 5 shows the image of the speckle pattern produced by flicking the toothbrush dipped in black paint.

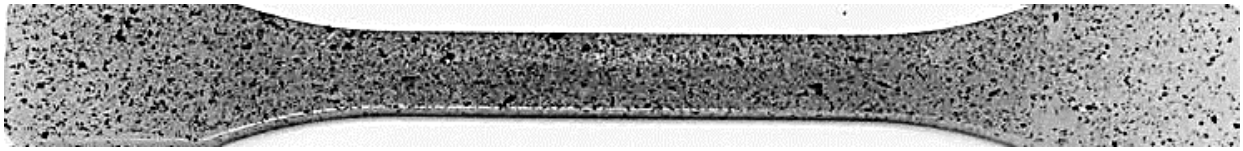

Figure 5: Speckle pattern generated by flicking a toothbrush

After generating the speckle pattern, it was discovered that the size of the speckle pattern was too big. To resolve this issue, the method of applying the paint to the specimens was changed to a spray paint because a smaller sized speckle pattern could be easily generated using the spray paint method.

It was observed that the speckle pattern generated using the spray paint had low contrast and the surface was reflective making it difficult to identify the speckle pattern when imaged. A matt white paint was first sprayed on the specimen to form a non-reflective base. A matt black spray paint was used to produce a fine random speckle pattern on the matt white base, thereby, creating an improved contrast between the speckle pattern and the base of the specimen. The next sub-section deals with the quality of speckle pattern.

3.2.1 Quality of speckle pattern

In the previous section, the methods used to produce speckle pattern on the HDPE specimens were discussed. In this section, the good and bad qualities of speckle pattern and ways to improve the quality will be discussed.

The success of the DIC technique depends on the quality of the speckle pattern. Speckle pattern consist of bad and good qualities.

The following are characters of a bad speckle pattern: low contrast, poor material-to-paint adhesion, big speckle size that leads to a subset filled by one colour and globally identical speckle pattern causing the subset to look identical. All the qualities listed above makes it difficult to track the subsets as the specimen is being loaded.

(a)

(b)

Figure 6: Images of a bad speckle pattern: (a) Low contrast and (b) Large speckle pattern size.

Figure 6 shows images of a bad speckle pattern. Figure 6(a) is an image of a poor contrast between the speckle pattern and the base. Figure 6(b) also shows an image of a poor

quality of speckle pattern because some of the speckle pattern were too large it will be difficult to tracking the subset.

The qualities of a good speckle pattern are: globally random and locally unique, fine size and good adhesion to the specimen.

A globally random and locally unique speckle pattern means the pattern should be unique within different sub-areas of the specimen. The unique sub-areas enable the DIC algorithm to easily match deformed subsets with subsets from the reference image. A fine size means the speckle size should be fine thereby creating a unique pattern within the subset. The speckle pattern should not also be too small to enable the camera to capture the images properly during deformation.

Good adhesion means the speckle pattern should be properly bonded to the surface of the test specimen so that it deforms as the test specimen deforms leading to accurate DIC results. An example of a good quality speckle pattern is shown in Figure 7.

Figure 7: Image of a good speckle pattern.

To further improve the quality of the captured image, fibre optic lamp with dual flexible light guides with focusing lenses and adjustable intensity was used during the test.

While carrying out the tensile test, it was observed that the paint had not properly adhered to the surface of the HDPE specimen due to the poor HDPE surface adhesion attribute,

therefore, needed improvement. The steps taken to improve the adhesion are discussed in section 3.2.2.

3.2.2 Improving HDPE surface adhesion

The quality of speckle pattern was previously discussed. In this section, ways to improve the adhesion between the specimens and paint will be discussed.

It is paramount that the adhesion between the specimens and the paint are good. DIC technique relies on tracking the speckle pattern on the images obtained from before and after deformation of the specimen. If good paint adhesion is not achieved the speckle pattern will detach from the material surface while during testing thereby giving false displacements and ultimately false strain results. An example of the poor adhesion between the paint and HDPE specimen is shown in Figure 8.

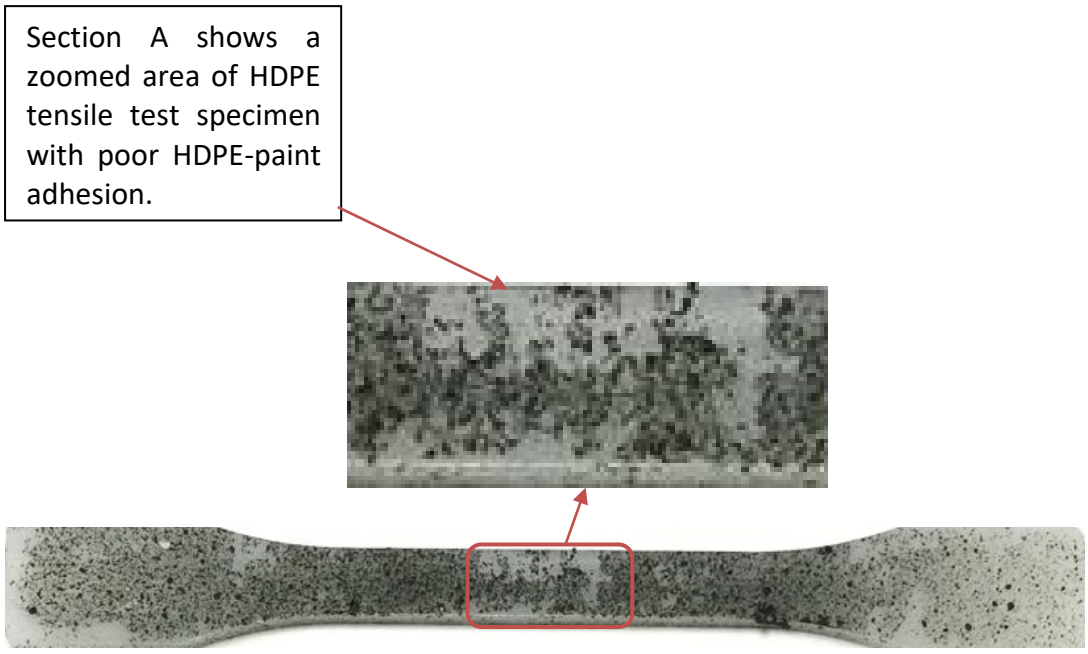

Figure 8: Poor HDPE-paint adhesion on tensile test specimen.

Various treatments were carried out in attempt to modify the surface of HDPE material before applying the paint to produce the speckle pattern for an improved HDPE-paint adhesion. The treatments are as shown in Table 3.

Table 2: Various surface treatment applied

Treatment	No surface treatment + white matt spray + black matt spray	Abraded + white matt spray + black matt spray	Flame treat + white matt spray + black matt spray
Paint adhesion	Poor	Poor	Good

From the analysis listed in Table 3, it was observed that abrading the surface of the material had no effect on the adhesion attribute of the material, however, flame treating the surface significantly improved the adhesion attribute of the material. In conclusion, the optimum solution was flame treating the HDPE material surface and then sprayed with matt white paint to form a non-reflective high contrast base. A matt black spray paint was used to generate speckle pattern and to avoid light reflection. An example of an improved HDPE-paint adhesion is shown in Figure 9. The effect of flame treatment on the material's mechanical properties is discussed in the following section.

Figure 9: Sample with improved adhesion between paint and HDPE after loading.

After the adhesive properties had been improved, tensile tests were carried out on HDPE specimens. Section 3.2.3 discusses the effect of flame treatment on the material.

3.2.3 Effect of flame treatment on polymer.

In the previous section, two methods were applied to improve the surface adhesion of the material and it was concluded that flame treatment was the optimum option.

In this section, the effect of flame treatment on mechanical properties of polymeric materials will be discussed.

Previous studies show that flame treatment is a common technique used in improving the wettability and adhesion of polymeric surfaces even for film materials where the thickness of the material is very small. These studies show that the material properties of the film materials were not affected as the wettability and adhesion properties of the material surface were enhanced using flame treatment, which is attributed to the oxidation of top surfaces of the material (<10nm) (Tuominen et al., 2013). The thickness of the specimens used in this study is considerably greater than that of the film materials and some comparative tests of flame treated and untreated were carried out on HDPE and these showed no observable effect on the mechanical properties.

3.3 Tensile testing of specimens

In the previous section, the effect of flame treatment on polymeric material was discussed as part of specimen preparation. After generating a good speckle pattern, the next stage was to subject the specimens to tensile load.

Tensile tests were carried out by clamping each specimen on both ends with serrated jaws in a sliding wedge grip and tensile load was applied at a strain rate of 0.83% per minute.

The test was limited to the linear region of the HDPE and GPPS material as shown in Figure 26 and figure 27 in Appendix B respectively.

3.4 Full-field displacement and strain using DIC

A camera was mounted on a stable tripod and positioned in front of the specimen. A two-dimensional DIC technique requires a single camera to capture the specimen. An image of the region to be analysed was captured before the load was applied to the specimen. Subsequent images were captured at force intervals of 20N up to a force of 560N. The camera resolution was set to 6,016 by 4000 pixels (pixels is the smallest unit of an image) covering the gauge length (60mm) of the specimen as shown in Figure 10.

At the end of the test, the images were transferred for post processing and it was observed that the images were moving erratically, contrary to what was expected. The erratic movements were caused by a combination of alignment issues in the grip and camera vibration which was not the case during testing. These issues were resolved by implementing the following steps.

The grips that were attached to the tensile machine were changed from serrated jaws in a sliding wedge to pneumatic grips with less sliding parts to eliminate the alignment issues. Also, the images were previously captured by pressing the shutter release button on the camera which contributed to the vibrations observed in the post processing stage. To avoid vibrations while capturing the images, a remote shutter/ trigger was used, and the camera's mirror was set to mirror up mode to further reduce vibrations.

During testing, the images need to be captured at the exact load and that could require holding the crosshead at a fixed force to capture the images. The challenge with holding the crosshead lies in the fact that HDPE material is visco-elastic. Due to the visco-elastic

property of the material, holding the crosshead of the tensile machine at a fixed force would not necessary prevent further deformation of the HDPE test specimen, which would lead to falsified displacement and strain readings. The strain rate was therefore set at a low rate of 0.83% per minute to allow images to be captured without stopping the crosshead. Table 7 in Appendix A contains the list of equipment used to conduct the DIC experiment.

3.4.1 Post Processing of Images

The previous section details how the images were captured, and the issues encountered with their solutions. This section describes how the images were processed using a Matlab algorithm.

The captured images were converted from the camera's raw format to Tagged Image Format (TIF). Using ImageJ software, the images were converted to grayscale, calibrated to enable further processing using DIC algorithm in Matlab.

The steps employed using DIC algorithm in Matlab are:

- Image setup
- Generate grid
- Correlation of images
- Compute
- Visualise results.

Firstly, image setup (using the command image_setup_GUI) was used to arrange the images into a sequence following the order they were captured and then saved as filenamelist. Within the image setup window, the format of the images was selected, and image skip was set to 1(means the images will be arranged in an increment of 1). Arranging

the images in the right order is important because if the order is wrong, the displacement and strain obtained will be wrong as well.

Secondly, a grid (an array of control points) was generated and superimposed on the reference image over a specified area to be correlated as represented by the blue region in Figure 10a. The immediate surrounding area of a control point is referred to as a subset.

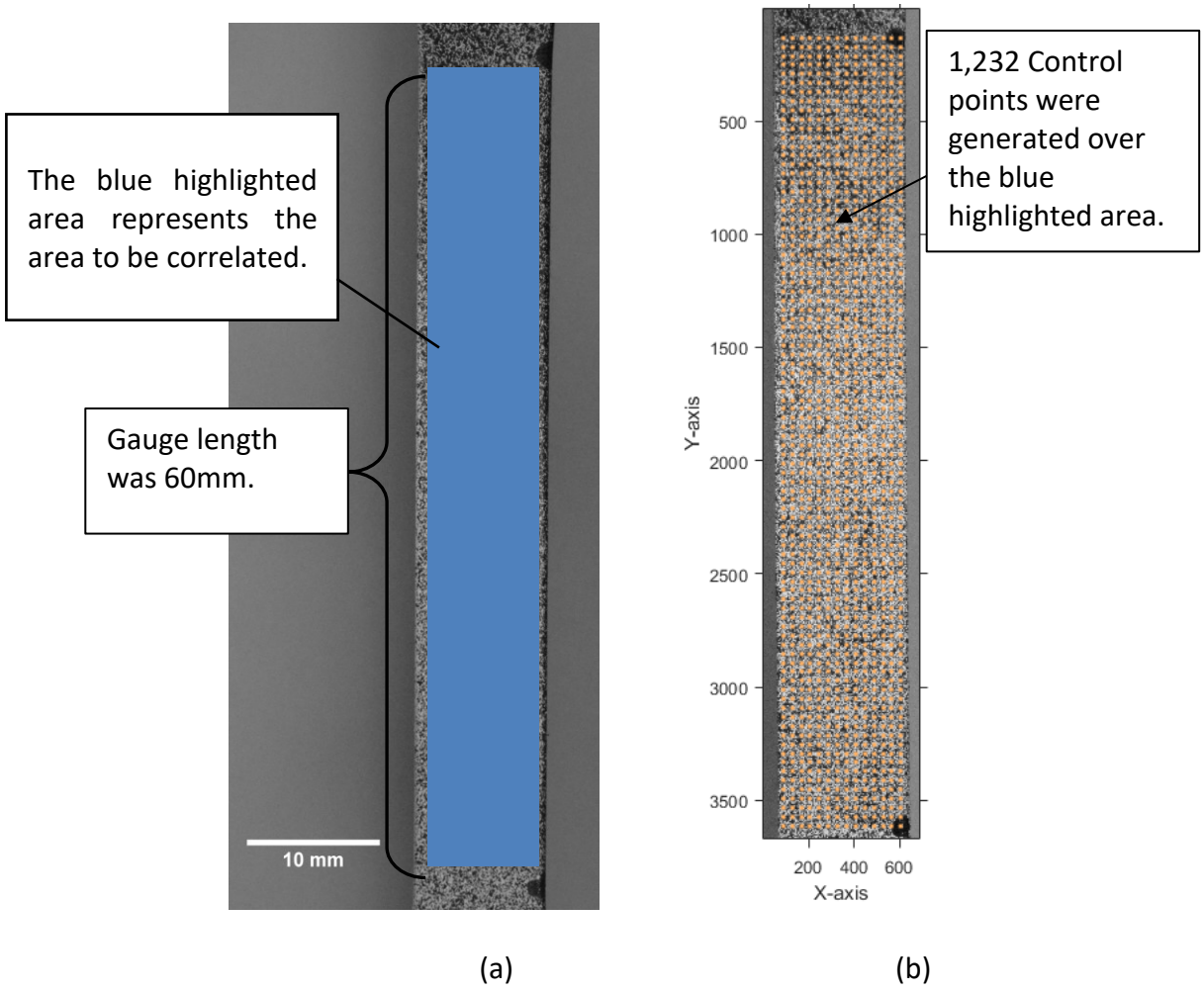

(a) (b)

Figure 10:(a) An example of scaled image with correlated area highlighted in blue, (b) An image of the control points over the selected area.

After the images were arranged as captured and grid was generated and superimposed on the first image as previously described. In this section, the correlation of the images will be discussed.

Thirdly, the images were correlated by using correlate_images_GUI command to define the correlation parameters. The first image was set as the reference image and full-sized images were correlated with a subset size (21), threshold (0.5) and a sparse grid (step size of 40). Correlation is done by tracking (searching for similar patterns in the subset of the reference image in subsequent images using the grayscale values) the subset of the reference image in subsequent images. The correlation algorithm computes the normalized cross-correlation coefficient, C, for a number of displacements *(u', v')* by a pixel increment.

$$\mathrm{C}\ (u', v') = \frac{\Sigma_{x',y'}\left[\left(r(x', y') - r^{-}{}_{u',v'}\right)(d(x' - u', y' - v') - d)\right]}{\{\Sigma_{x',y'}\left[\left(r(x', y') - r^{-}{}_{u',v'}\right)^2\right]\left[\left(d(x' - u', y' - v') - d\right)^2\right]\}^{1/2}} \qquad equation\ 1$$

Where r is the intensity of the pixels in the reference subset, d is the intensity of the pixels in the deformed subset, (x', y') are the local subset coordinate axes located at the centre of the control point and (u', v') is the theoretical displacement.

Displacement plots were obtained to determine how well the images were correlated and if initial guesses are required using reduced-sized images.

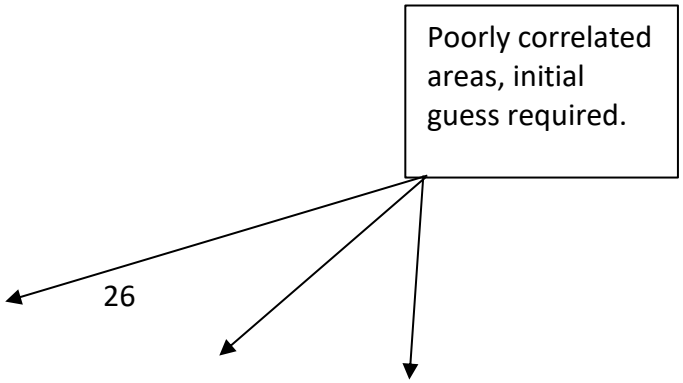

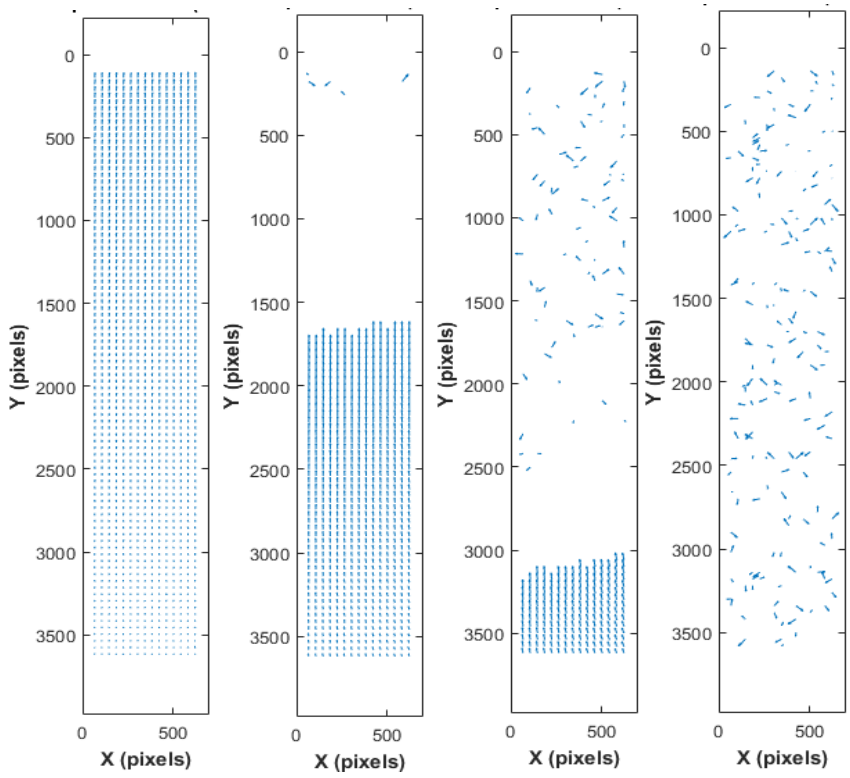

(a) (b) (c) (d)

Figure 11: Vector field of displacement.

Figure 11(b)-(d) shows that the images were not well correlated due to large displacement, therefore, initial guesses are needed. Correlation of reduced-sized images was implemented by using an image reduction factor of two to scale down the full-sized images, thereby generate initial guesses. It was found that by increasing the subset size to 91 pixels the images were better correlated as shown in Table 4. The optimum correlation setting was subset size of 91, threshold of 0.9 and step size of 20.

Table 3: Subset optimisation for reduced images correlation

Reduced image correlation										
Subset size	21	41	61	81	91	91	91	91	91	91
Threshold	0.5	0.5	0.5	0.5	0.5	0.3	0.5	0.7	0.9	0.95
Step size	20	20	20	20	20	20	20	20	20	20

After the reduced images were correlated, the full-sized images were correlated using the data obtained from the reduced image correlation (as initial guesses). The displacement results were generated to determine how well the full-sized images were correlated. After well-correlated images were obtained, the threshold was then altered to further improve the results as shown in Table 5. The optimum setting was subset size of 91, threshold of 0.9 and step size of 40.

Table 4: Optimisation of threshold

Full image correlation					
Subset size	11	21	21	91	91
Threshold	0.5	0.5	0.8	0.9	0.95
Step size	40	40	40	40	40

3.4.1.1. Assessment of correlated images

This section describes how the correlated images were accessed.

Initially, vector field plots were used to access the correlated images, however, as the magnitude of the displacement increases, the size of the vectors overlaps each other and thereby covering the areas that are not well correlated. Contour plots were used to access the plots with high magnitude of displacements occurring. Contour plot is a better method of assessing how well the images are correlated because the colours do not overlap unlike

vector field plots where the vectors overlap each other at high magnitude of displacement as seen in Figure 12.

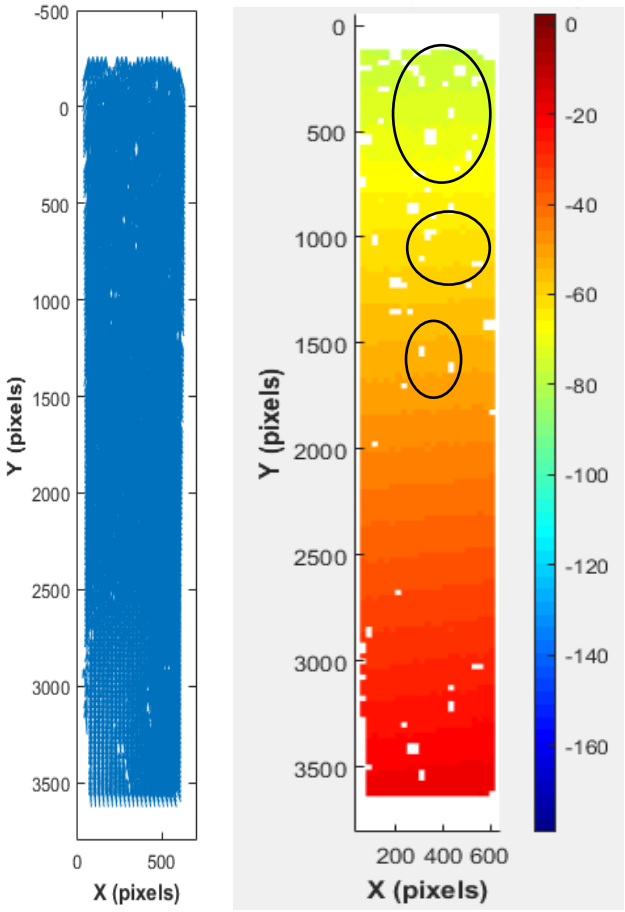

(a) (b)

Figure 12: (a) and (b) Vector and Contour plot of image 20 respectively.

Fourthly, the compute data command was used to smoothen the displacement by applying a gaussian distribution of weights to the control points and strain was computed.

Finally, the visualize command was used to display the results of the DIC analysis done. The results can be plotted in contour or a vector form.

Chapter 4 Results of DIC technique.

In this chapter, the results from DIC analysis will be presented. The results from DIC technique for HDPE will be presented followed by the results from DIC technique for GPPS specimens.

4.1 Results of DIC technique using HDPE specimens

In this chapter, results of the test conducted on HDPE test specimen such as displacement, longitudinal strain, transverse strain and Poisson ratio obtained from the DIC will be presented and discussed in the following sections.

The longitudinal and transverse strain was used to obtain the Poisson's ratio and the test was repeated for sixteen specimens made from the same batch of material used in the investigation.

4.1.1 Displacement plots.

Displacement results were obtained from the correlation of the images using the matlab algorithm as previously stated. The displacement results were presented in vector field plots.

An example of the displacement plot over a selected correlated region is shown in

Figure 13. In Figure 13, the vectors represent the magnitude and direction of the displacement within the correlated area of the test specimen. The vertical direction of the vectors shows that the material was subjected to tensile load, which agrees with the physical observation during the experiment. The size of the vectors increases as the magnitude of the displacement increases, which is as a result of increase in load. The

magnitude of the vectors is greater at the upper area compared to the lower area within the correlated region.

Images similar to that presented in Figure 13 were also obtained from sixteen test specimens that were tested and analysed using the DIC technique.

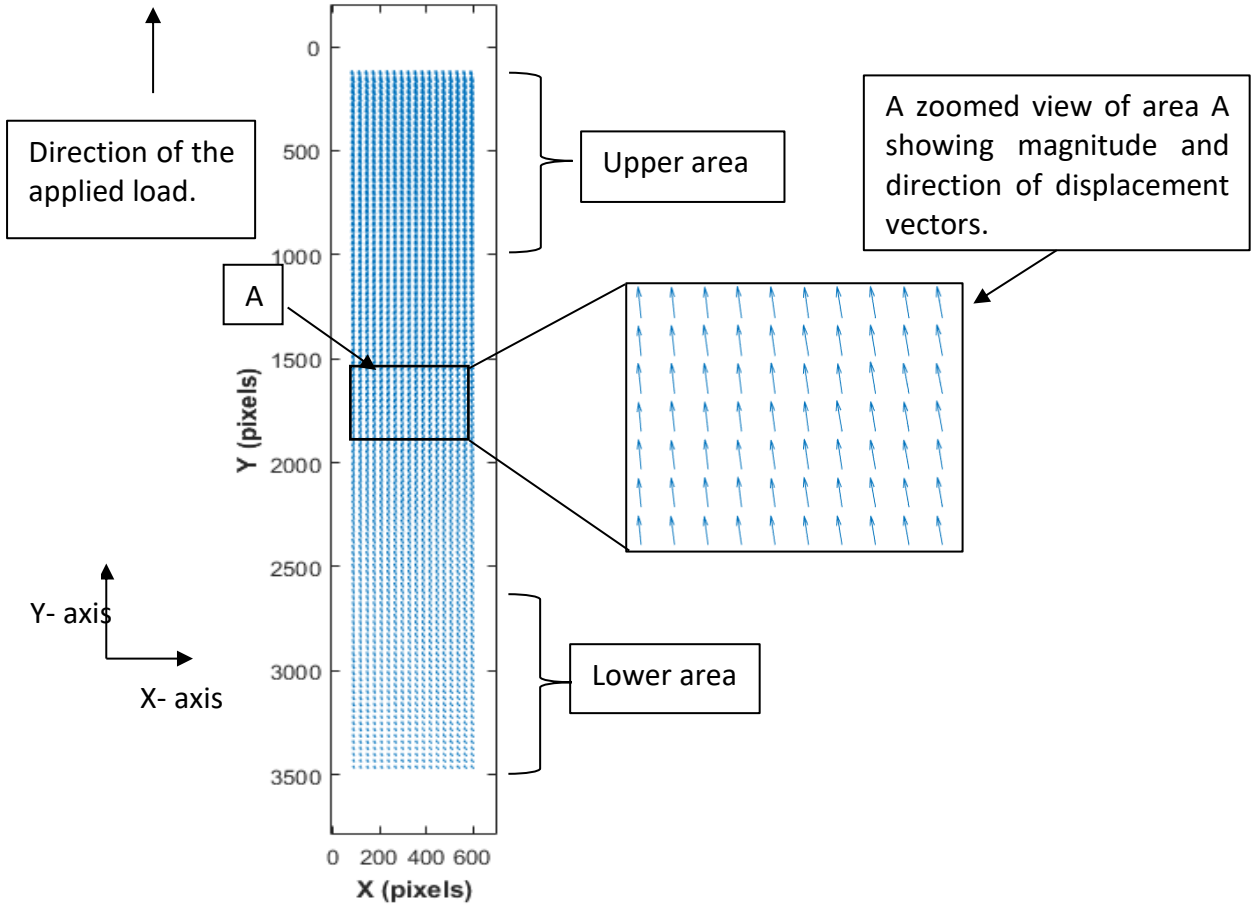

Figure 13: Vector field of displacements at 80N over an area (60mm x 10mm).

4.1.2 Longitudinal strain (e_{yy})

In the previous section, the displacement was obtained by correlating the images. This section will be focused on the longitudinal strain (strain acting in the direction of the applied force) results**.** Figure 24(a)-(e) show plots of e_{yy} at the subset within the correlated

region of the images that were captured at loads of 0N, 140N, 280N, 420N and 580N. The first image (at 0N) shows zero percent strain because the first image was self-correlated without any load applied. Figure 14(a) to (e) showed variation in longitudinal strain across the test specimen as the load increased. The e_{yy} plots were plotted in different suitable scales in order to show the variation in strain within the image.

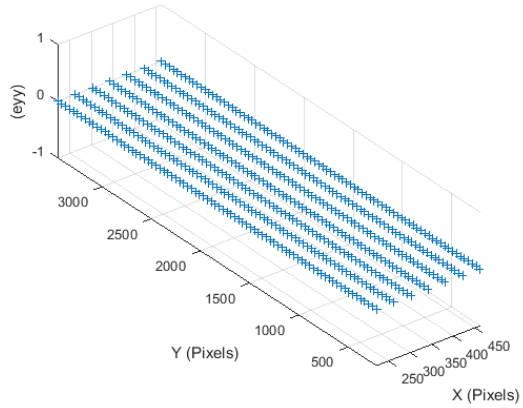

(a) e_{yy} at a Force of 0(N)

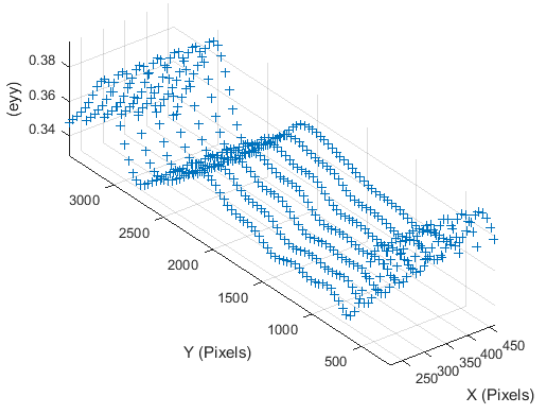

(b) e_{yy} at a Force of 140(N)

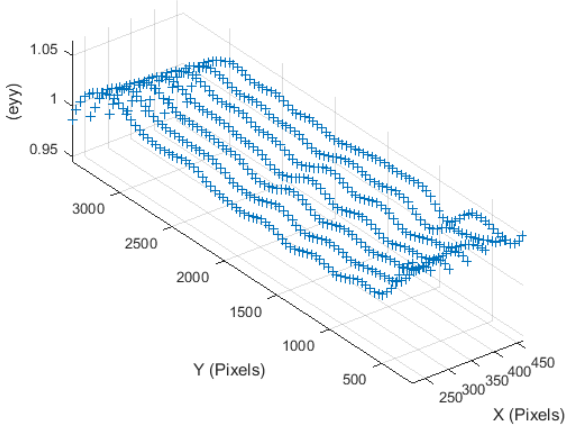

(c) e_{yy} at a Force of 280(N)

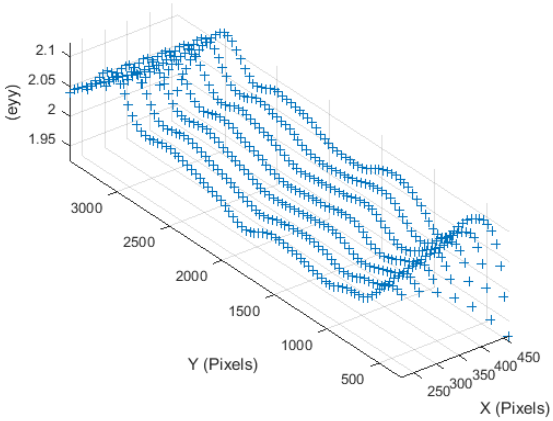

(d) e_{yy} at a Force of 420(N)

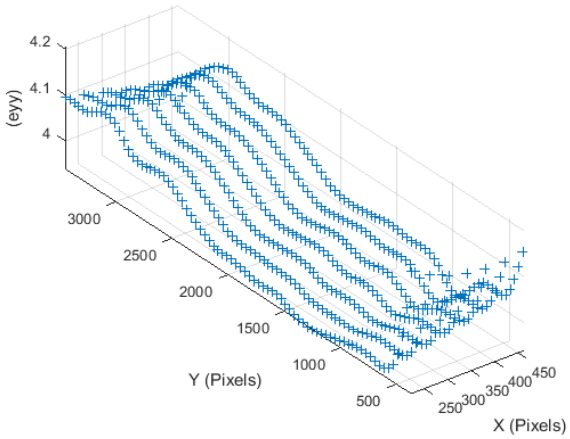

(e) e_{yy} at a Force of 560(N)

Figure 14(a) – (e): Longitudinal strain map using the control points at different force for a single test specimen.

4.1.3 Transverse strain (e_{xx})

In the previous section, longitudinal strain results obtained by correlating the images were presented. This section will be focused on the transverse strain (strain acting in the perpendicular direction to the applied force) results.

Figure 15 show e_{xx} plots within the correlated region of the images captured at load of 0N, 140N, 280N, 420N and 580N. Similar to the longitudinal strain, the first image should show zero percent transverse strain because it was self-correlated and no load was applied to the test specimen at the time. The transverse strain plot also showed non-uniformity in strain across the test specimen, which implies that deformation was non-uniform across the test specimen.

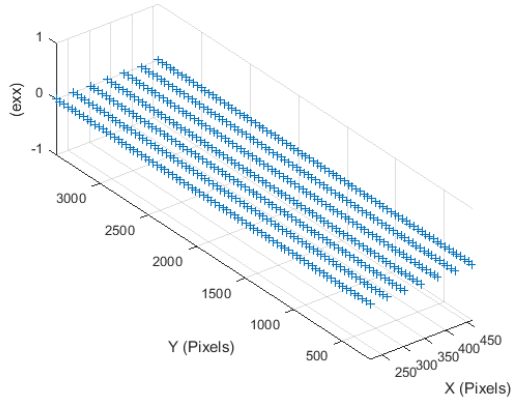

(a) e_{xx} at a Force of 0(N)

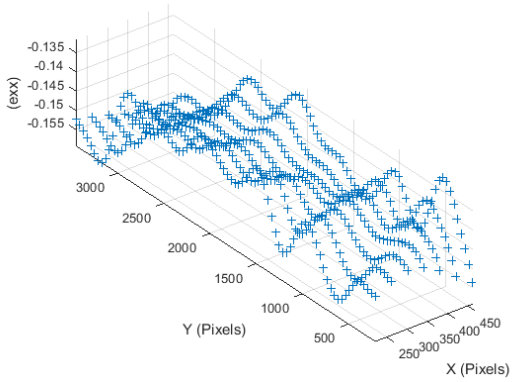

(b) e_{xx} at a Force of 140(N)

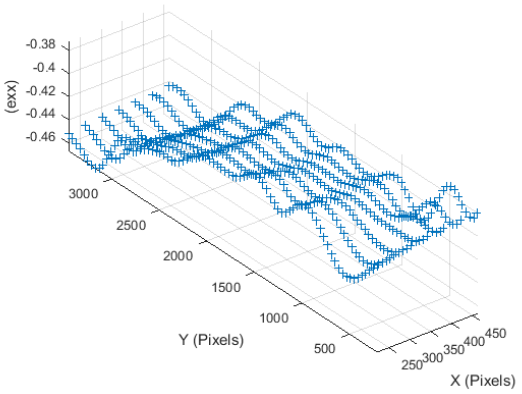

(c) e_{xx} at a Force of 280(N)

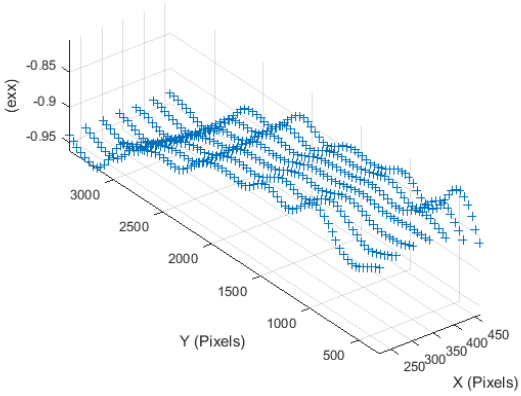

(d) e_{xx} at a Force of 420(N)

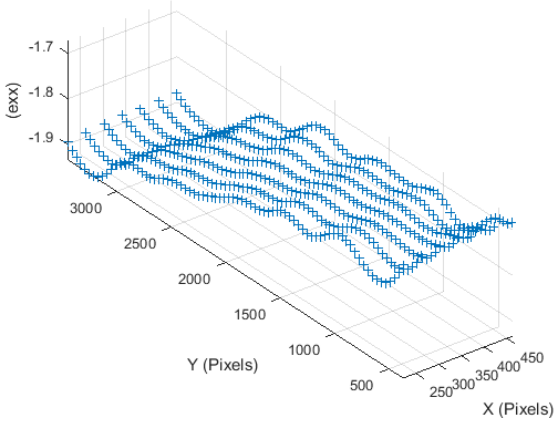

(e) e_{xx} at a Force of 560(N)

Figure 15: Transverse strain map using the control points at different force for a single test specimen.

4.1.4 Reducing the noise in the data

Gaussian distribution of weights was applied to the data in order to smooth the data at the subset level against noise inherent to the data, hence the strains obtained were averaged over each subset in the correlated area. The kernel size of the control point was used in the smoothening process as well as the weighting function. When the Gaussian distribution of weights is applied, the displacements at control points within the kernel are weighted with a Gaussian distribution centred at the central control point and then averaged.

4.1.5 Longitudinal and transverse strain evolution

In this section, both longitudinal and transverse strain history will be presented within each image as the load increases from 0N to 560N. Figure 16 show plots of Longitudinal and transverse strain evolution.

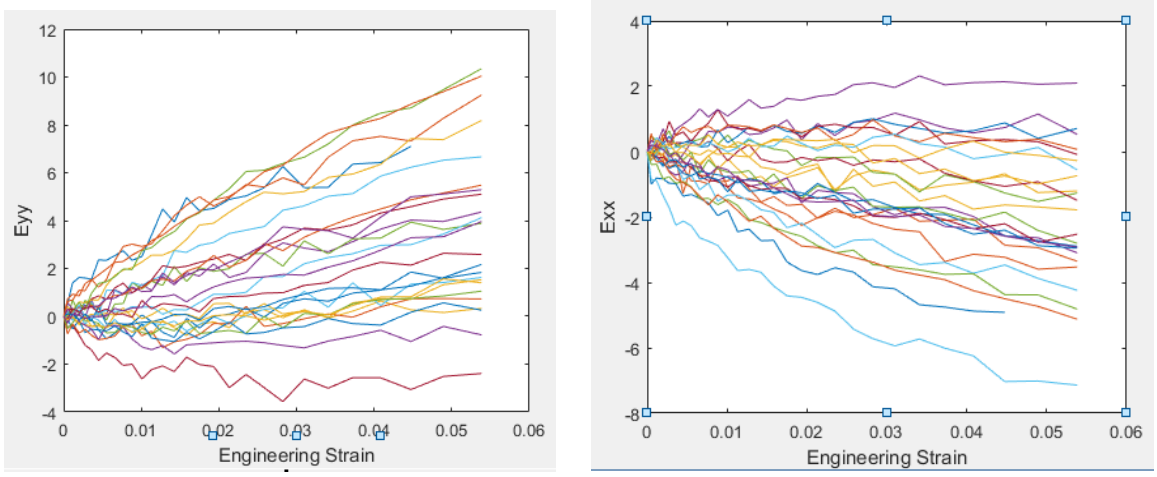

(a) (b)

Figure 16: (a) e_{yy} against nominal strain and (b) e_{xx} against nominal strain.

Figure 16(a) and (b) shows longitudinal and transverse strain evolution respectively for twenty-five control points as the nominal specimen strain increases. Figure 16(a) shows that most control points increasingly strained in the positive e_{yy} direction, which suggests that the material in that area expanded, however, some subsets were increasingly strained in the negative e_{yy} direction, which suggests that compression occurred. In Figure 16(b), most of the subsets were negatively strained thereby indicating that compression occurred in the transverse direction. Some control points were positively strained indicating the material in that area expanded.

A possible explanation could be that as the test specimen was subjected to tensile stress, expansion occurred longitudinally within the material. The expansion then may have resulted in a local compression within the material. Similarly, compression in the transverse direction may have resulted in a local expansion occurring in the transverse direction. As a result of the semi-crystalline nature of the material, compressive or tensile force may cause the molecules (especially the amorphous region) to be displaced from their initial or intended position. This displacement could be in any direction, thereby producing a positive or negative strain effect.

4.1.6 A combined Poisson's ratio plot for sixteen HDPE test specimens

In the previous section, longitudinal and transverse strains were obtained and presented. This section is focused on the Poisson's ratio and its evolution of the correlated area.

Poisson's ratio is defined as the negative ratio of transverse strain to longitudinal strain. Poisson's ratio was calculated using the strain values within the correlated area of the

images. The evolution of Poisson’s ratio was then plotted against strain for the sixteen test specimens.

As previously stated, sixteen tests were conducted and each of these tests contains twenty-nine images. Images were captured at different loads ranging from 0N to 560N, with an increment of 20N. Each subset within the correlated image contains a control point that acts like a sensor; that stores data such as displacement, longitudinal strain or transverse strain.

An average transverse strain history was obtained by averaging all the control points of each image for each specific load. Similarly, an average longitudinal strain history was obtained by averaging all the control points of each image at specific loads. An averaged Poisson’s ratio was then obtained from the negative ratio of the average transverse to average longitudinal strain.

Figure 17 shows sixteen curves representing the Poisson's ratio history of sixteen different test specimens produced from the same batch of material. The markers represent the average Poisson’s ratio at that load and are linked with either a continuous or broken line as shown in Figure 17. As the strain increases, the curves showed a converging pattern as seen in Figure 17.

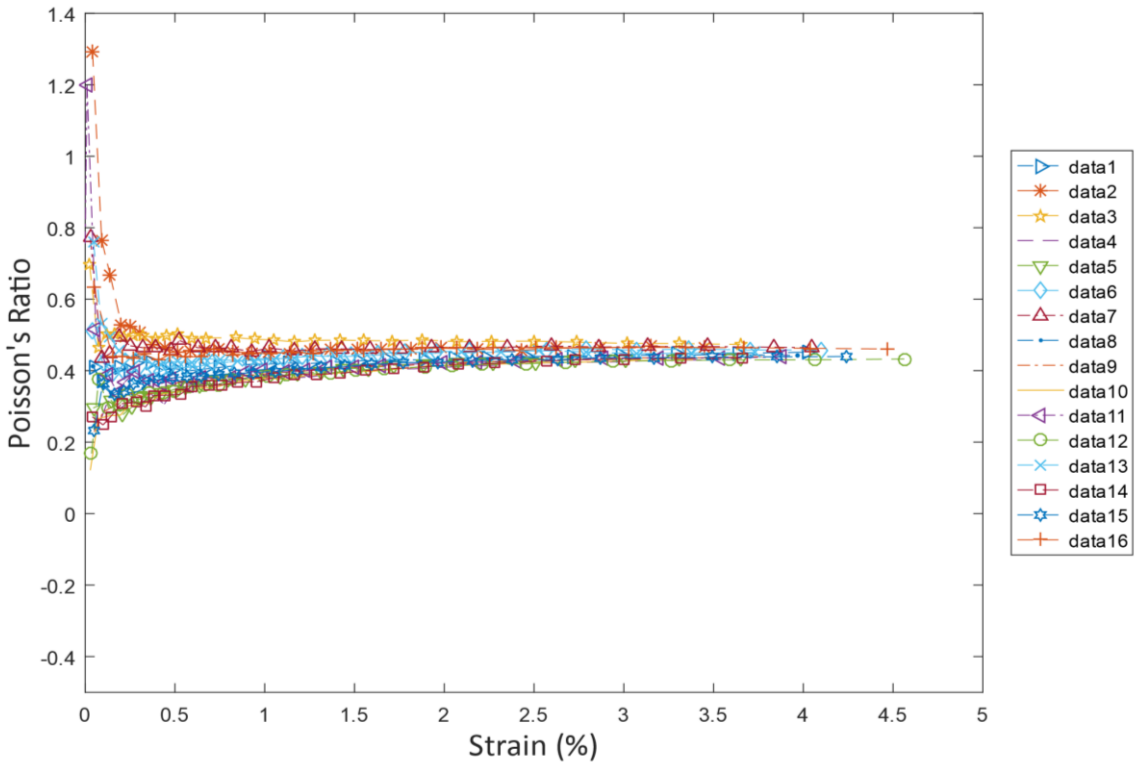

Figure 17: Poisson's ratio history for sixteen HDPE specimens.

4.1.7 Poisson's ratio for a single specimen

Previously, Poisson's ratio history was obtained and presented for sixteen different specimens of the same batch of materials. In this section, the Poisson's ratio of a single specimen will be obtained and presented so as to closely examine the strain behaviour.

Figure 18 shows a plot of Poisson's ratio against strain for a single test specimen. Furthermore, Figure 18 also show twenty-nine sets of strain field represented by colours, each represents the twenty-nine images captured during the tensile test and correlated with the DIC algorithm using the preceding image as the reference image.

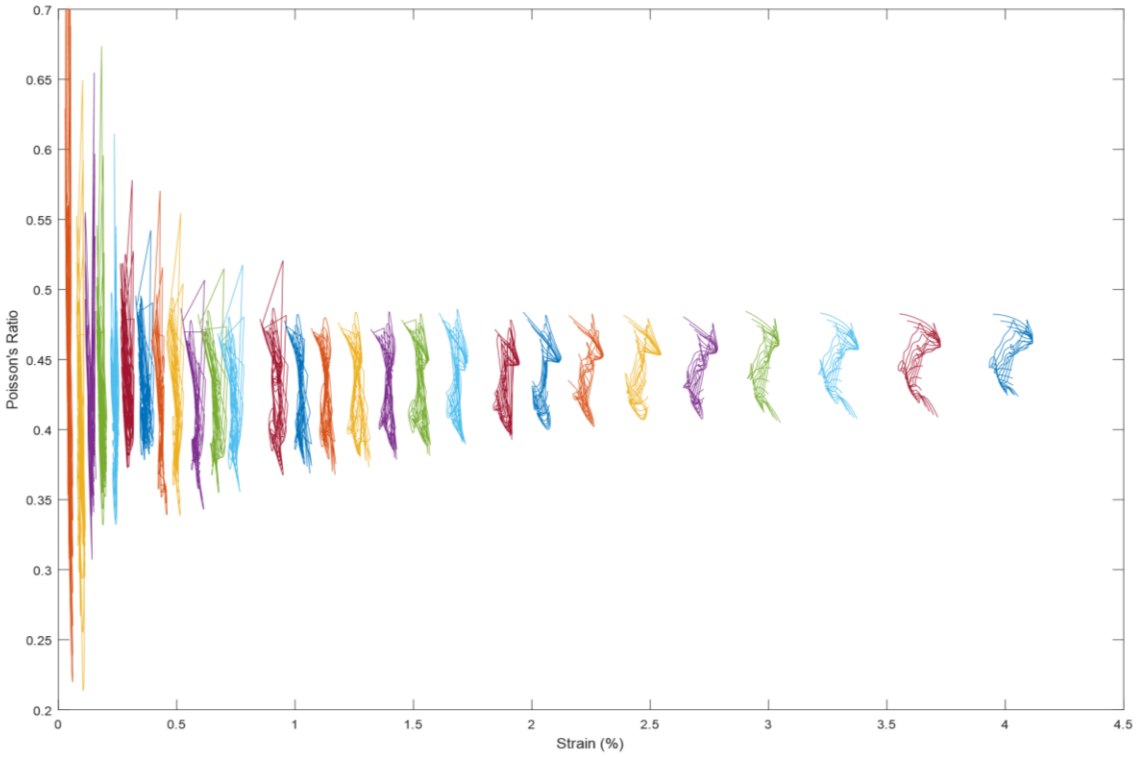

Figure 18: Poisson's ratio against strain of HDPE specimen.

From Figure 18, each strain field also showed variation in Poisson's ratio and in the strain as the HDPE deforms. As the strain increases, the shape evolves from a vertical thin region to a horizontal wide region. At low strain (below 1% strain) the variation in strain is minimum, however, the variation in Poisson's ratio is high. As the strain increases (above 1% strain), the variation in strain increases while the variation in Poisson's ratio decreases. Figure 18 also presents the evolution of Poisson's ratio within each image in relation to strain. At low strain of about 0 to 1%, Poisson's ratio was inconsistent: where some points within the image were higher than the theoretical values of Poisson's ratio for this material, however, as the strain increases, the material deforms further and the Poisson's ratio gradually stabilised as it approaches 5% strain.

4.2 Results of DIC technique using GPPS specimens

In this chapter, the results of the tensile tests conducted on GPPS specimens such as longitudinal strain, transverse strain and Poisson's ratio obtained using DIC technique will be presented and discussed in the following sections.

The longitudinal strain and transverse strain were used to obtain Poisson's ratio and the test was repeated for sixteen specimens made from the same batch of material used in the investigation.

4.2.1 Longitudinal strain (e_{yy})

This section will be focused on the longitudinal strain (strain acting in the direction of the applied force) results**.** Figure 14(a)-(e) show contour plots and a three-dimension map of e_{yy} at the subset within the correlated region of the images. The images were captured at loads of 0N, 140N, 280N, 420N and 580N. The first image (at 0N) shows zero percent strain because the first image was self-correlated without any load applied. Figure 14(b)-(e) showed variation in longitudinal strain across the test specimen as the load is increased. The e_{yy} plots were plotted in different suitable scales to show the variation in strain within the image.

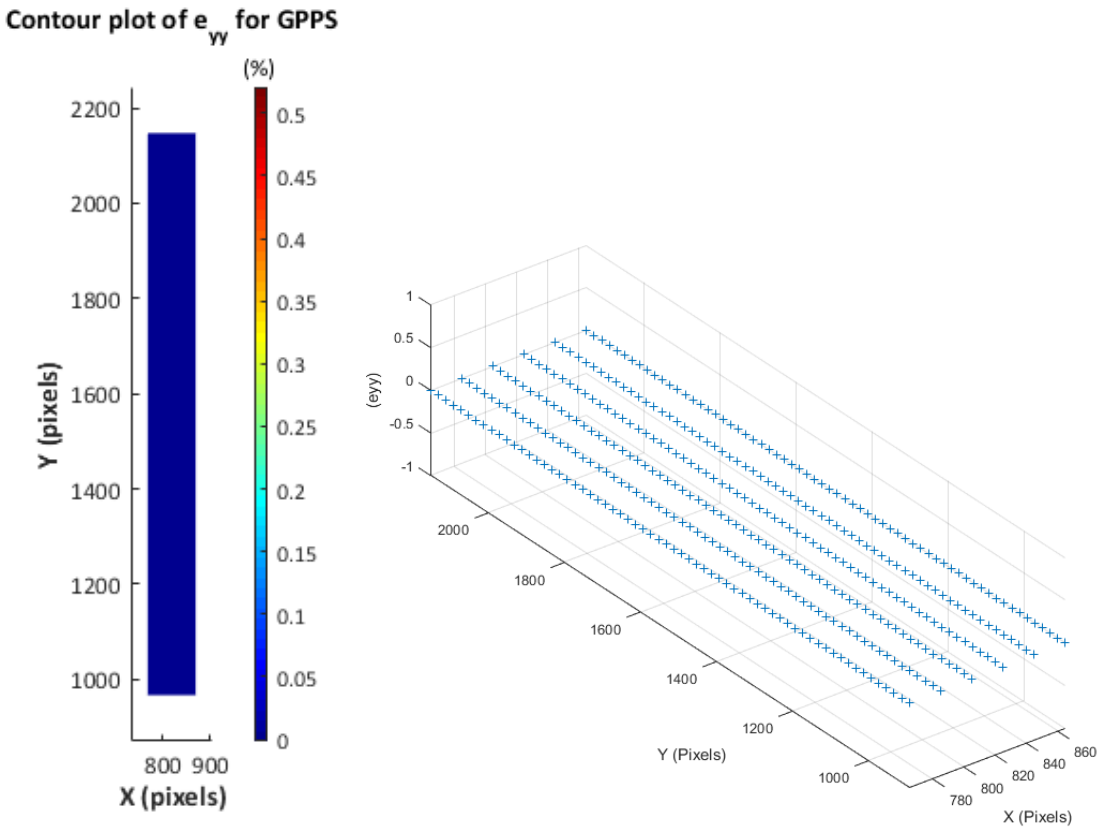

(a) Contour plot of e_{yy} and subset map of e_{yy} at a Force of 0N

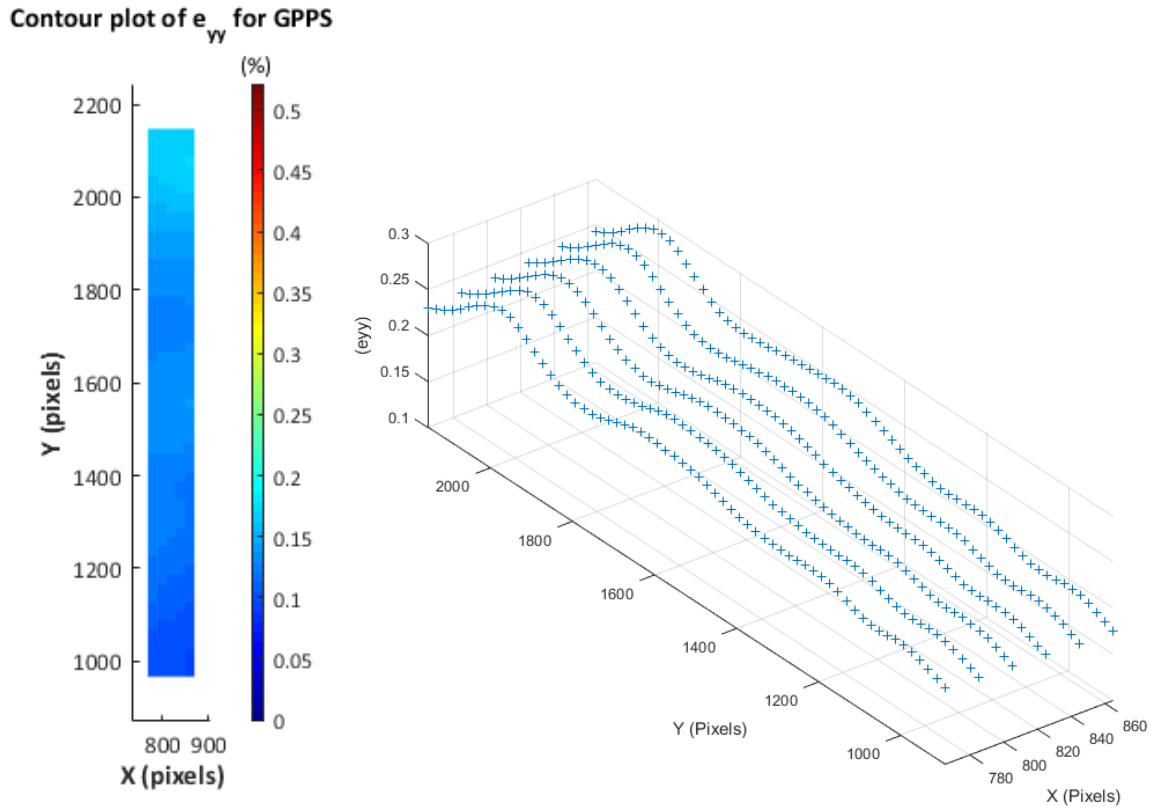

(b) Contour plot of e_{yy} and subset map of e_{yy} at a Force of 140(N)

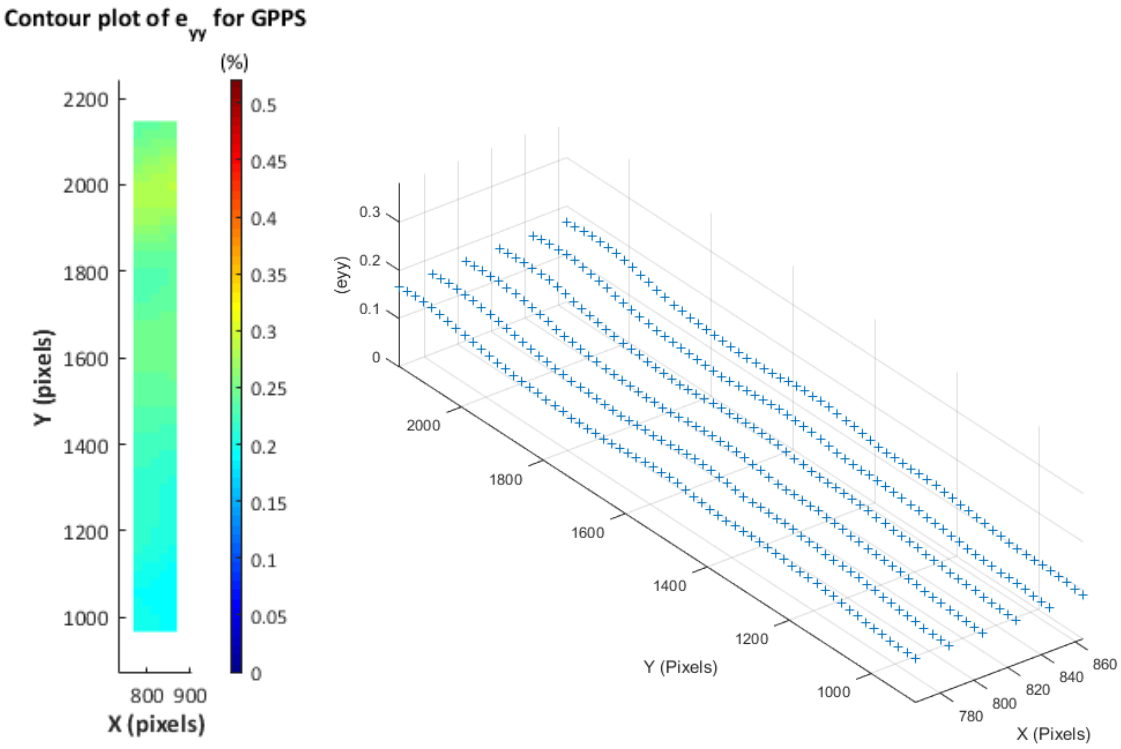

(c) Contour plot of e_{yy} and subset map of e_{yy} at a Force of 280(N)

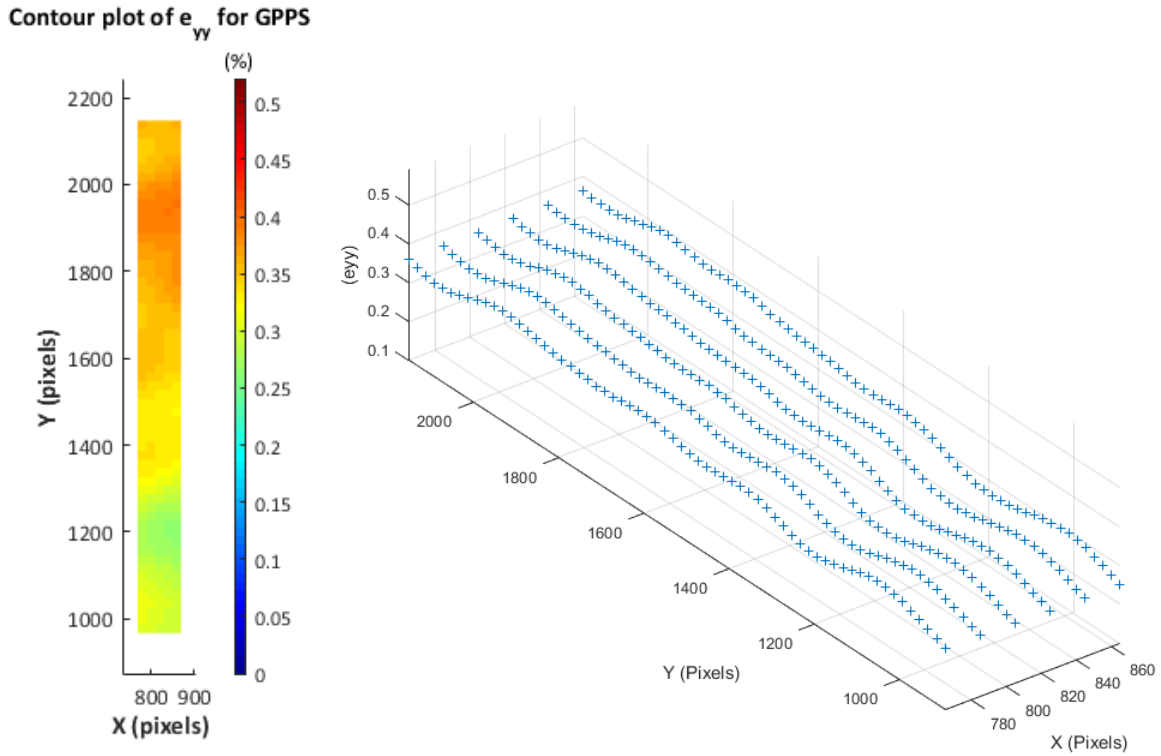

(d) Contour plot of e_{yy} and subset map of e_{yy} at a Force of 420(N)

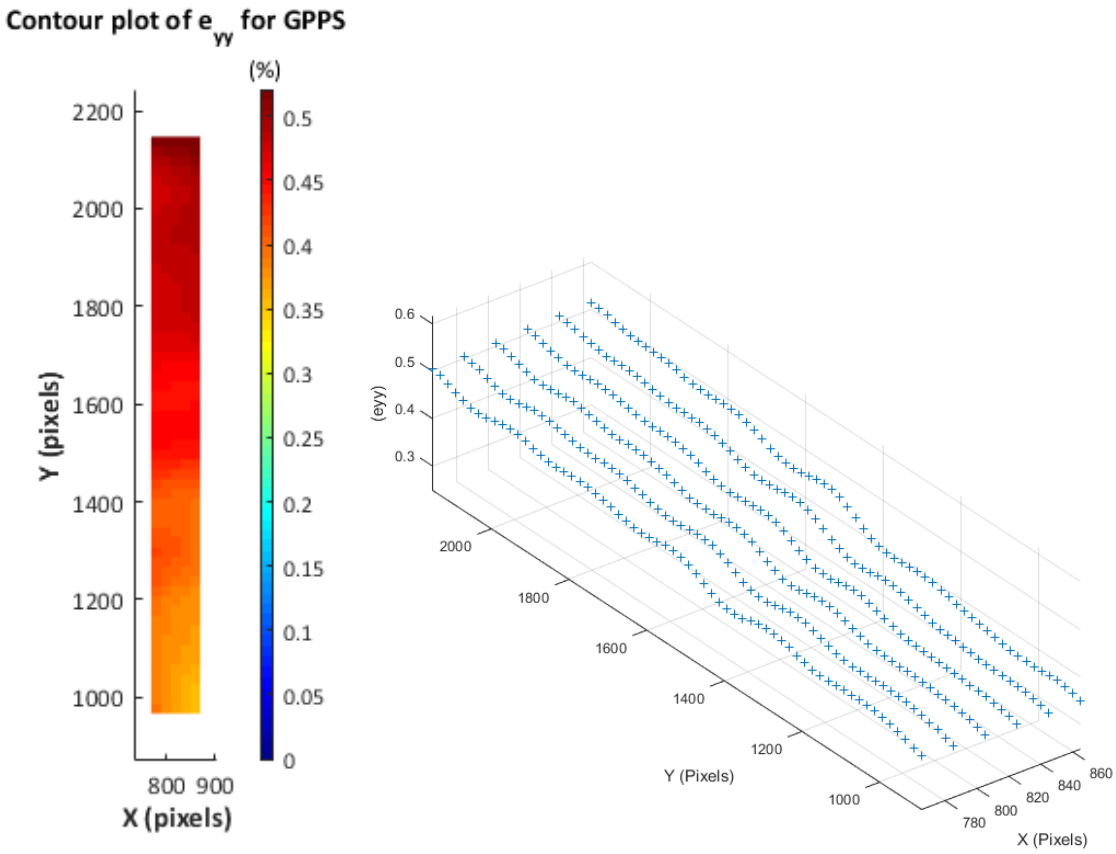

(e) Contour plot of e_{yy} and subset map of e_{yy} at a Force of 560(N)

Figure 19(a) – (e): Contour plot and longitudinal strain map using the control points at different force for a single GPPS specimen.

4.2.2 Transverse Strain (e_{xx})

In the previous section, longitudinal strain results obtained by correlating the images were presented. This section will be focused on the transverse strain (strain acting in the perpendicular direction to the applied force) results.

Figure 20 show contour plots and subset e_{xx} plots within the correlated region of the images captured at load of 0N, 140N, 280N, 420N and 580N. Similar to the longitudinal strain, the first image should show zero percent transverse strain because it was self-correlated and no load was applied to the test specimen at the time. The transverse strain

plot also showed non-uniformity in strain across the test specimen, which implies that deformation was non-uniform across the test specimen.

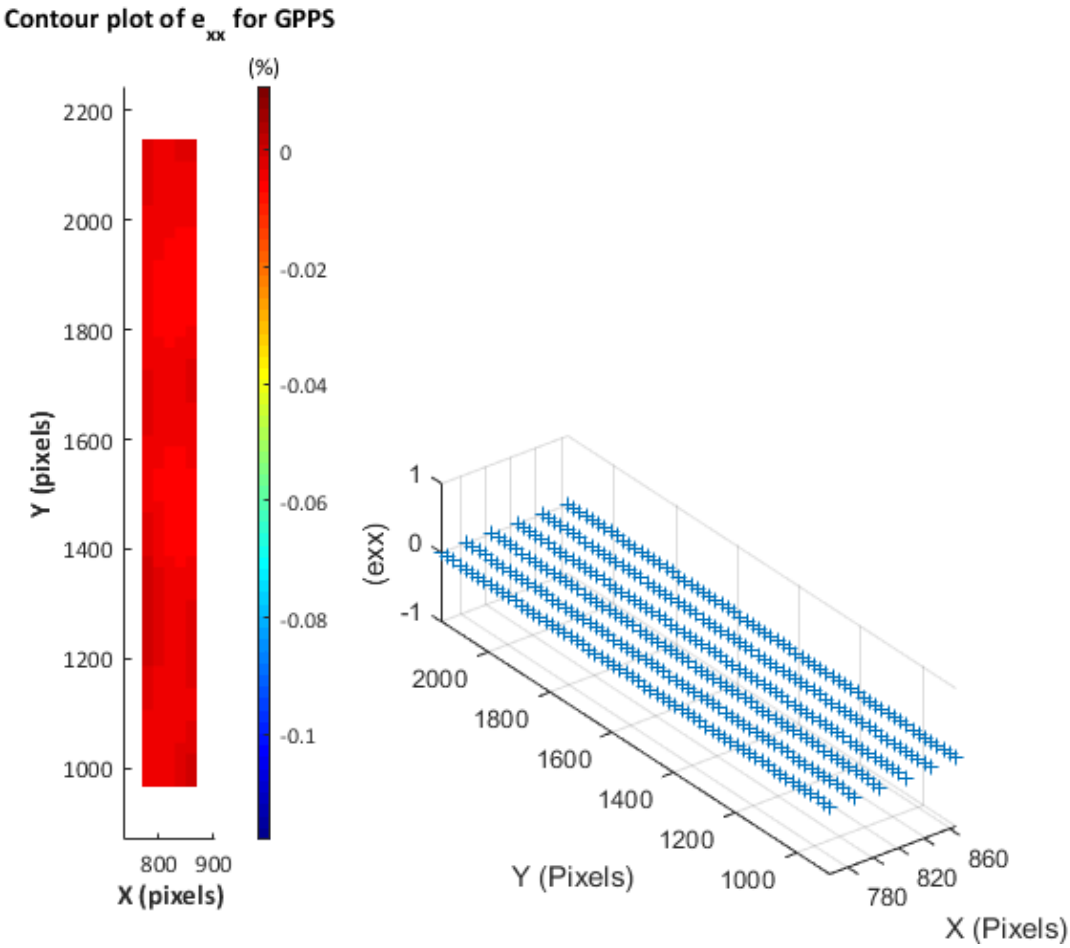

(a) Contour plot of e_{xx} and subset map of e_{xx} at a force of 0N

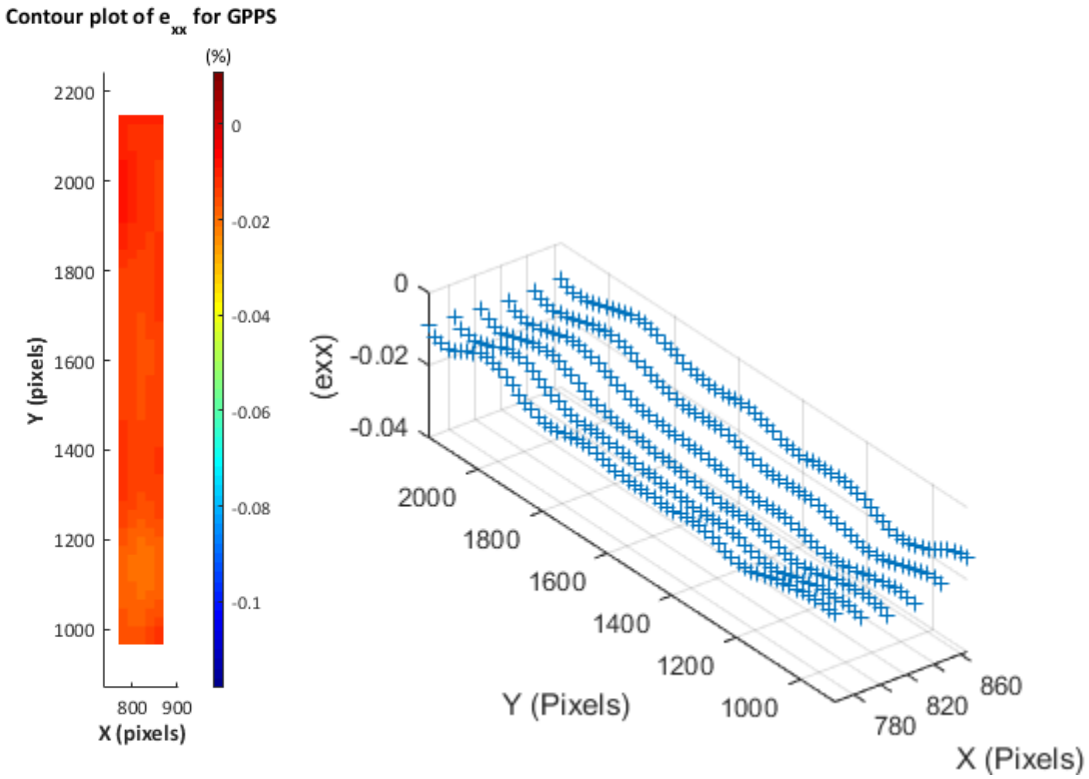

(b) Contour plot of e_{xx} and subset map of e_{xx} at a force of 140N

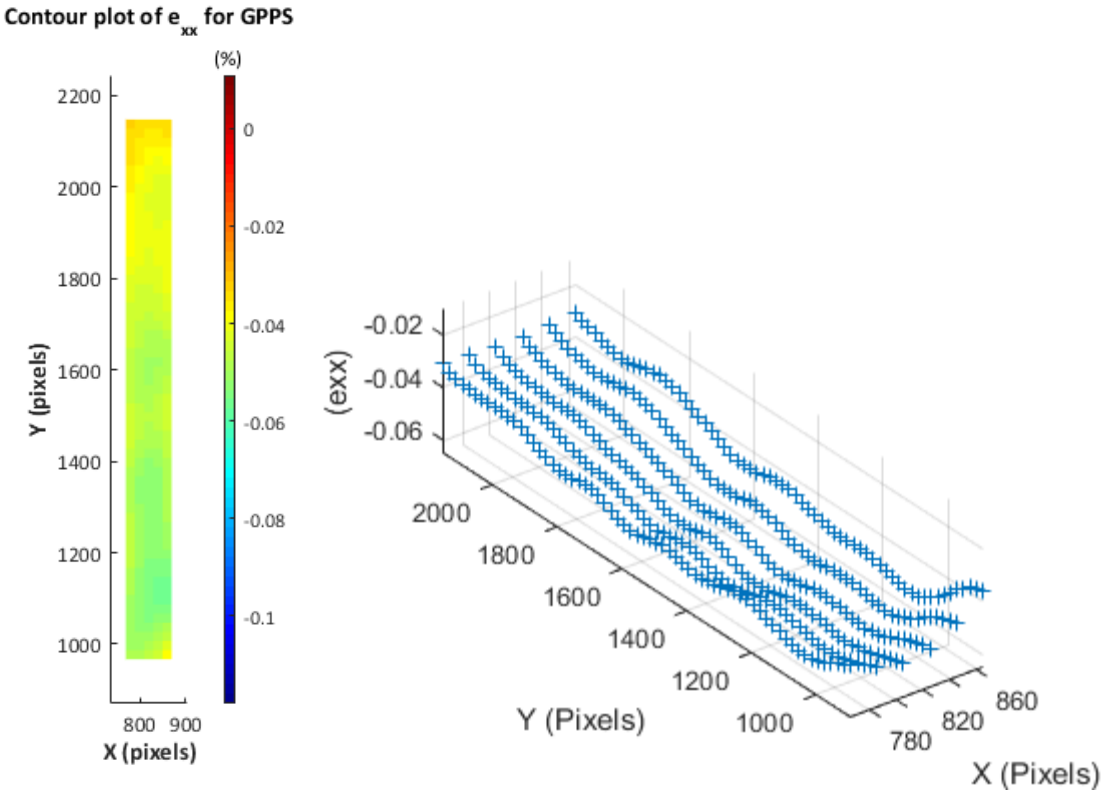

(c) Contour plot of e_{xx} and subset map of e_{xx} at a force of 280N

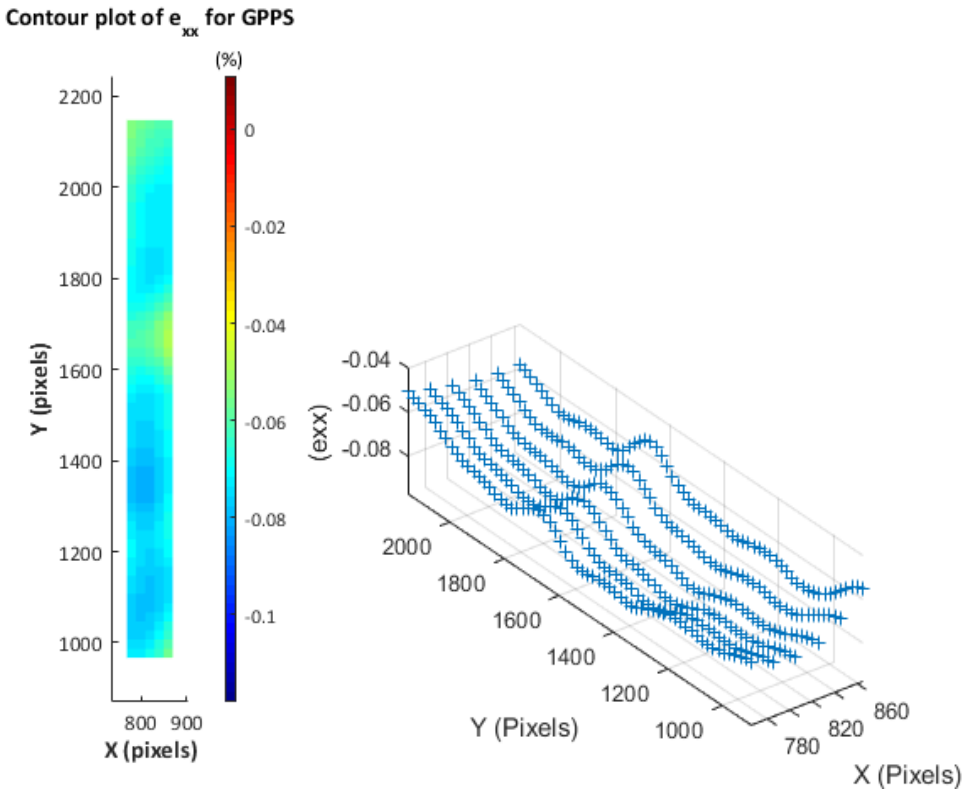

(d) Contour plot of e_{xx} and subset map of e_{xx} at a force of 420(N)

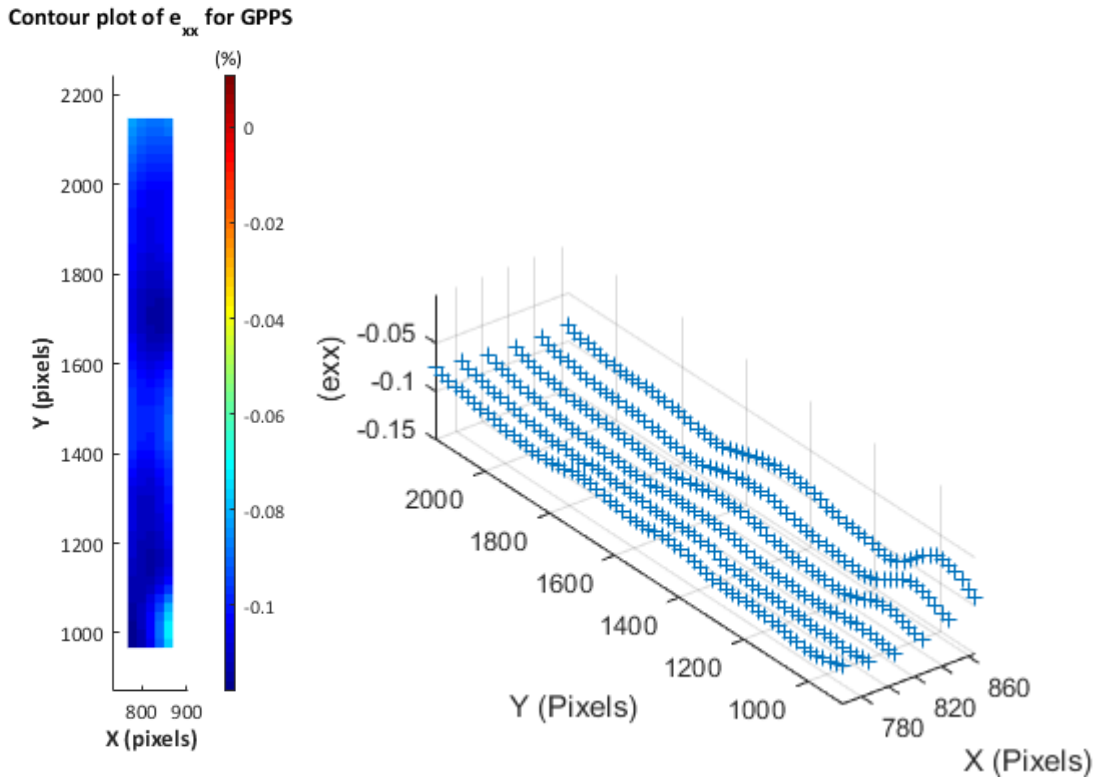

(e) Contour plot of e_{xx} and subset map of e_{xx} at a Force of 560(N)

Figure 20: Transverse strain map using the control points at different force for a single GPPS specimen.

Appendix C shows a table of the Force, extension, engineering stress and engineering strain.

4.2.3 Reducing the noise in the data

Gaussian distribution of weights was applied to the data in order to smooth the data at the subset level against noise inherent to the data as discussed in section 4.1.4.

4.2.4 Longitudinal and transverse strain evolution

In this section, both longitudinal and transverse strain history will be presented within each image as the load increases from 0N to 560N. Figure 21 show plots of Longitudinal and transverse strain evolution.

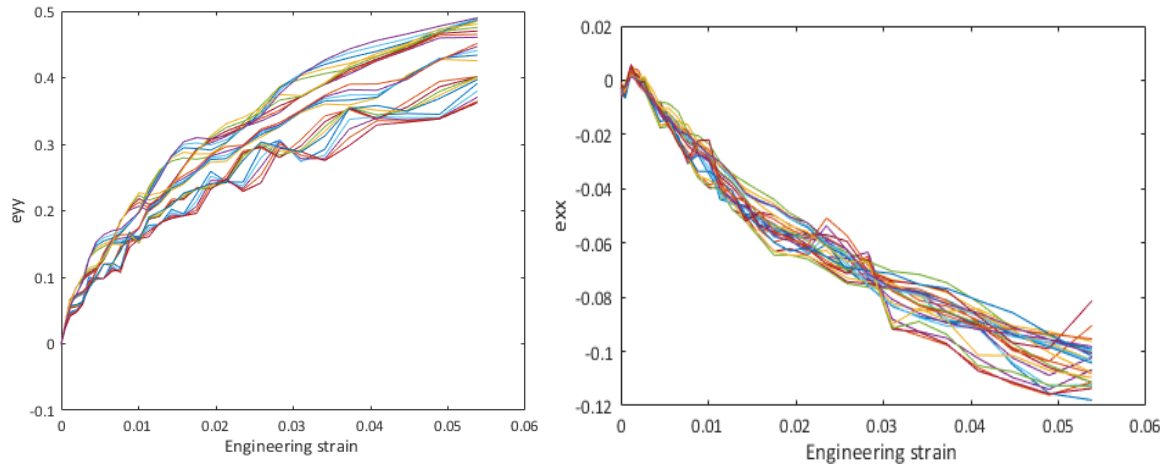

(a) (b)

Figure 21: (a) e_{yy} against nominal strain and (b) e_{xx} against nominal strain.

Figure 21(a) and (b) shows longitudinal and transverse strain evolution respectively for twenty-five control points as the nominal specimen strain increases. Figure 21(a) shows that the GPPS specimen increasingly strained in the positive e_{yy} direction, which suggests that the material in that area is expanded. In Figure 21(b), the GPPS specimen was

negatively strained thereby indicating that compression occurred in the transverse direction. This is as expected when a material is subjected to tensile load.

4.2.5 A combined Poisson's ratio plot for fourteen GPPS test specimens

In the previous section, longitudinal and transverse strains were obtained and presented. This section is focused on the Poisson's ratio evolution over the correlated area.

Poisson's ratio is defined as the negative ratio of transverse strain to longitudinal strain. Poisson's ratio was calculated using the strain values within the correlated area of the images. The evolution of Poisson's ratio was then plotted against engineering strain.

Fourteen tests were conducted and each of these tests contains twenty-nine images. Images were captured at different loads ranging from 0N to 560N, with an increment of 20N. Each subset within the correlated image contains a control point that acts like a sensor; that stores data such as displacement, longitudinal strain or transverse strain.

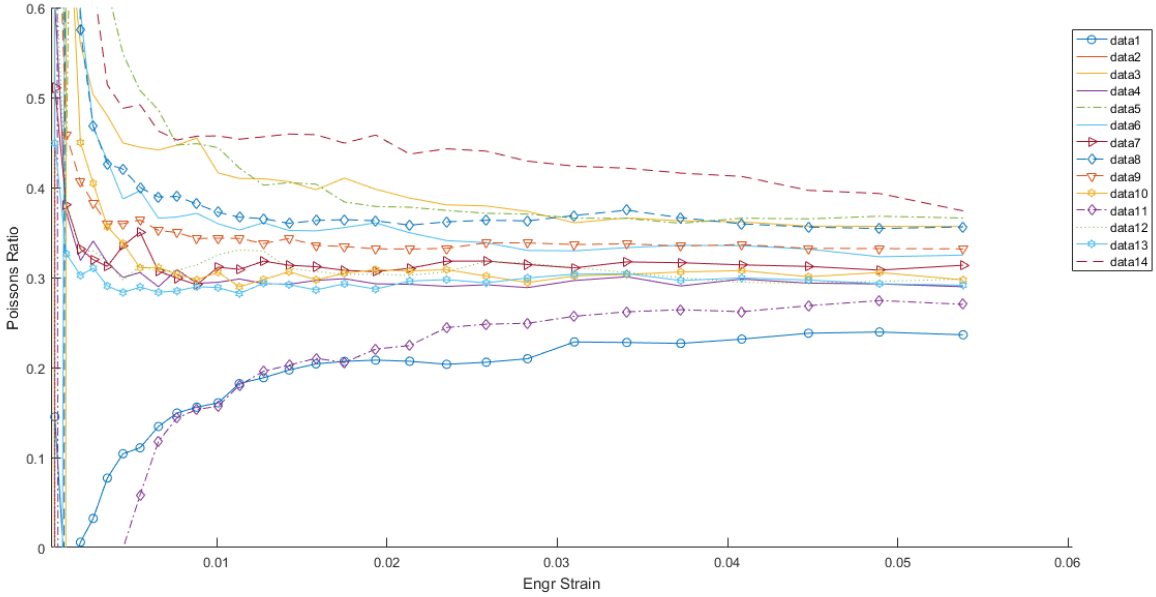

Figure 22: Poisson's ratio history for sixteen specimens.

An average transverse strain history was obtained by averaging all the control points of each image for each specific load. Similarly, an average longitudinal strain history was obtained by averaging all the control points of each image at specific loads. An averaged Poisson's ratio was then obtained from the negative ratio of the average transverse to average longitudinal strain.

Figure 22 shows fourteen curves representing the Poisson's ratio history of sixteen different test specimens produced from the same batch of material. The markers represent the average Poisson's ratio at that load and are linked with either a continuous or broken line as seen in Figure 22. As the strain increases, the curves showed a converging pattern as seen in Figure 22.

4.2.6 Poisson's ratio for a single specimen

Previously, Poisson's ratio history was obtained and presented for sixteen different specimens of the same batch of materials. In this section, Poisson's ratio of a single specimen will be obtained and presented so as to closely examine the strain behaviour.

Figure 23 shows a plot of Poisson's ratio against strain for a single test specimen. Furthermore, Figure 23 shows twenty-nine sets of strain field represented by colours, each represents the images captured during the tensile test and correlated with the DIC algorithm using the preceding image as the reference image.

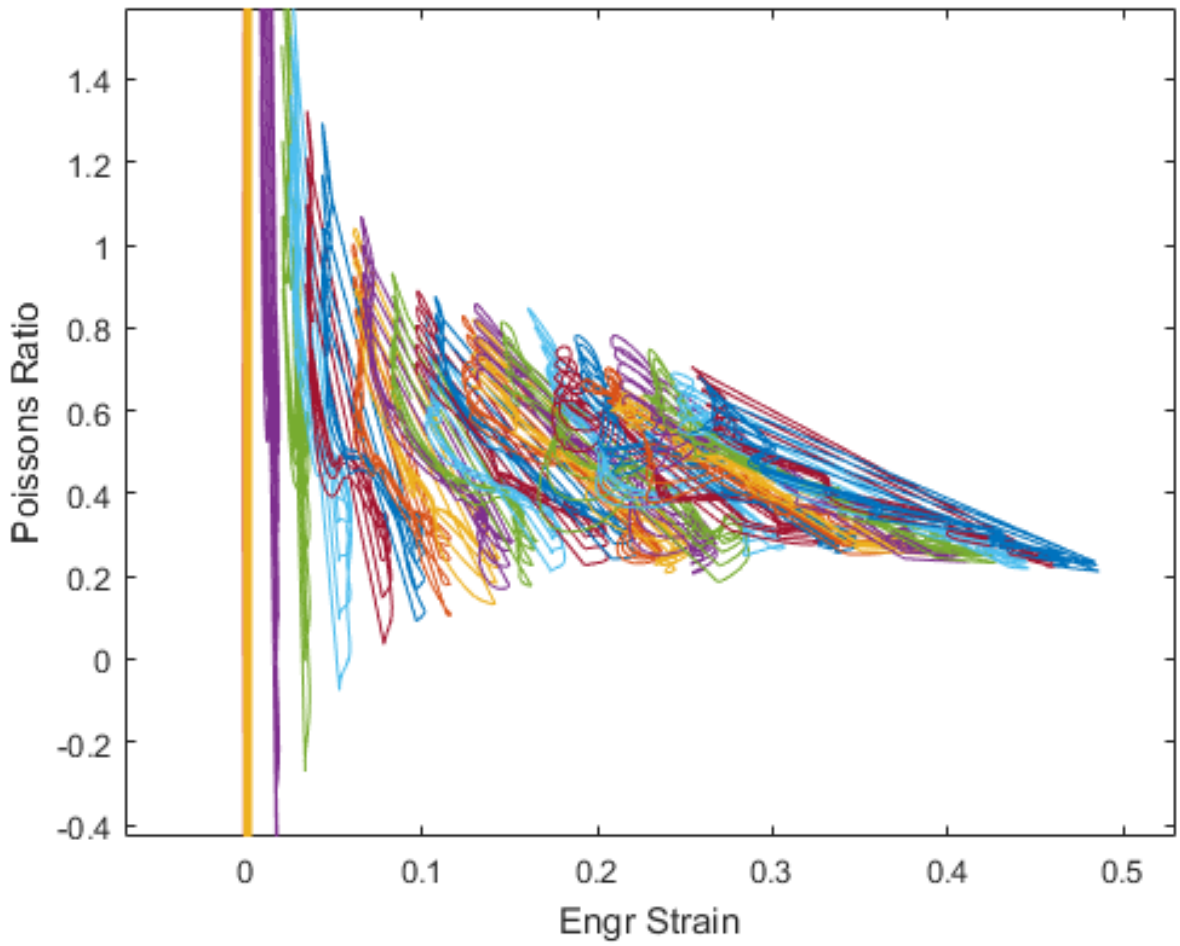

Figure 23: Poisson's ratio against strain for a GPPS specimen.

From Figure 23, each strain field also showed variation in Poisson's ratio and in the strain as the HDPE deforms. As the strain increases, the shape evolves from a vertical thin region to a horizontal wide region. At low strain (below 1% strain) the variation in strain is minimum, however, the variation in Poisson's ratio is high. As the strain increases (above 1% strain), the variation in strain increases while the variation in Poisson's ratio decreases. Figure 23 also presents the evolution of Poisson's ratio within each image in relation to strain. At low strain of about 0 to 1%, Poisson's ratio was inconsistent: where some points within the image were higher than the theoretical values of Poisson's ratio for this

material, however, as the strain increases, the material deforms further and the Poisson's ratio gradually stabilised as it approaches 5% strain.

4.3 Discussion of DIC results for HDPE specimen.

In the previous section, results of displacement, longitudinal strain, transverse strain and Poisson's ratio obtained from the DIC technique were presented. This section is focused on discussing the results in detail. A summary of the material used in the investigation will be initially discussed.

HDPE is a semi-crystalline polymer with crystalline regions surrounded by amorphous regions (Callister and David, 2010). Most polymers such as HDPE and Polypropylene have low surface adhesion as a result of the material's poor surface properties. It was observed during the testing of the HDPE specimen that the paint applied did not adhere to the surface of the material as the tensile test specimen was deformed, which may lead to invalid results. Methods to improve the surface adhesion of the material were implemented such as roughening the surface of the material and flame treating the surface of the material. After a series of tests, it was concluded that flame treatment was more effective over the other method as indicated in literature. The next stage was generating speckle pattern on the surface of the specimen.

Speckle pattern was generated initially using a brush technique by immersing the brush in black paint and flicking the brush in order to project the paint unto the specimen. The brush method was replaced by spray paint as the spray paint produced finer quality of speckle pattern. Low contrast and reflective surface were also observed due to the translucent nature of the material. The solution to the low contrast and reflective images

produced, was to first apply a matt white paint and then use a matt black paint to generate the speckle pattern.

Tensile tests were conducted at a constant strain rate of 0.83% per minute (test speed of 0.5mm/min) in order to capture the images at the desired load. The images are then processed using the DIC algorithm. The displacement obtained from the DIC test of the correlated area was determined and was used to visually validate the experimental process by generating and comparing the vector plot with the direction of the experiments. The displacement was also used to obtain the strain within the correlated area. The longitudinal and transverse strain plots were obtained and presented in the results section. Figure 16 shows an uneven distribution of both longitudinal and transverse strain respectively for HDPE specimen as the strain increases from 0 to 560N. The variation in longitudinal and transverse strain, which was also observed on the surface of sixteen different specimens tested could be attributed to the structure of the material.

As the specimen undergoes tensile stress, the material should be in tension in the direction of the applied force. Figure 16 shows some few subsets within the correlated area of the specimen had negative longitudinal strain, which indicates that compression occurred at those subsets as the specimen was strained. Most subsets within the correlated area had positive longitudinal strain, which indicates tension occurred at those subsets. In the transverse strain plot, the specimen is expected to undergo compression, however, few subsets had positive strain values within the correlated area, which implies that tension occurred at those subsets as the material was strained as shown in figure 16. Most subsets had negative strain as expected, which means that compression occurred at most subsets. The average strain (longitudinal and transverse) was obtained by averaging all the subsets

of the specimen. The average strain (longitudinal or transverse) plot is either positive or negative depending on if the subsets are mostly positive or negative.

The Poisson's ratio history for the tested HDPE specimen as shown in Figure 17 indicates that under 1% strain the Poisson's ratio is inconsistent but as the strain increases towards the yield point the Poisson's ratio stabilises.

The non-uniformity could be attributed to the structure of the material while subjected to tensile load. The tests were carried out to ensure that there was no external vibration as earlier explained in 3.4.

HDPE material deforms differently when strained at higher strain rates compared to low strain rate of 0.83% per minute (i.e test speed of 0.5mm/min). At low strain rates such as 0.83% per minute, the molecules in the amorphous region have more time to align and reposition while at higher strain rate, the molecules in the amorphous region have little or no time to align in the direction of the applied force. At low strain, elastic deformation occurs due to the elongation of the molecules. As the material deforms further, the molecules in the amorphous region experience changes in orientation and length. As the material continues to deform, the amorphous molecules are subject to align in the direction of the applied tensile load and may start to increase in crystallinity, which can be referred to as strain induced crystallinity. Further increase in strain will instigate an irreversible deformation of the molecular chains due to increased crystallinity.

4.3.1 Comparison of results obtained from HDPE and GPPS using DIC.

In this section, a direct comparison of both techniques used, and their results will be discussed.

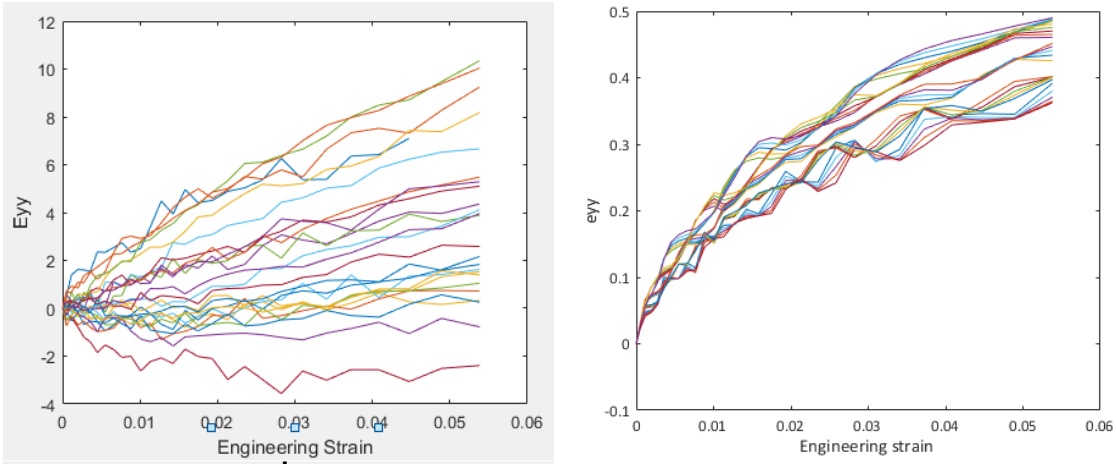

(a) (b)

Figure 24: (a) eyy for a single HDPE specimen and (b) eyy for a single GPPS specimen.

All specimens (HDPE and GPPS) were tested with the same strain rate and within the same region as previously stated. Figure 24 shows most subsets within the correlated area had positive longitudinal strain, which indicates tension occurred at those subsets of the HDPE specimen. Some few subsets, however, within the correlated area of the specimen had negative longitudinal strain, which indicates that compression occurred potentially at those subsets as the specimen was strained. In the GPPS specimen, all the subsets of the specimen were in tension as shown in Figure 24(b), which could be as a result of the material consisting of only amorphous structure.

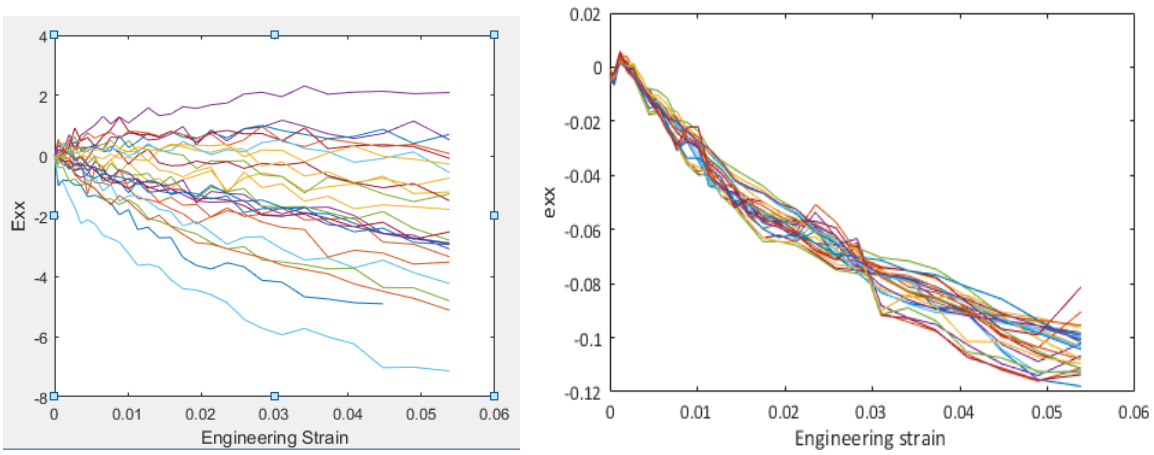

(a) (b)

Figure 25: (a) exx for a single HDPE specimen and (b) exx for a single GPPS specimen.

Figure 25(a) shows that most subsets within the correlated area had negative transverse strain, which indicates compression occurred at those subsets of the HDPE specimen as expected. Some subsets, however, had positive strain values within the correlated area, which implies that expansion occurred at those subsets as the HDPE material was strained. The expansion in the transverse direction observed in the case of HDPE may be related to rotation of some of the blocks of lamellae. Figure 25(b) shows that most subsets within the correlated area had negative transverse strain within the GPPS specimen.

Chapter 5 Conclusions

5.1 Conclusion

This thesis reported the work carried out to investigate the variation in Poisson's ratio as strain is applied to tensile test specimens, as reported in the literature (Bhabha, 2015). Using the DIC technique the variation in Poisson's ratio was clearly observed, particularly at low strains (below 1% strain), and the results obtained in this study were seen to be very similar to those previously reported.

HDPE and GPPS injection moulded test specimens produced from the Injection moulding machine (Battenfeld machine) were subjected to tensile testing using the Hounsfield (H10KS) tensometer. The surface displacement was measured using the DIC technique and the result was used to generate strain and Poisson's ratio map over an area.

The variations in Poisson's ratio were observed to be greatest at low strains. The variation in Poisson's ratio reduces as the strains increases. It was also interesting to note that as the specimen strain increased (and the value of Poisson's ratio decreased), the local longitudinal strain (e_{yy}) was observed to increase in value. These observations were confirmed over several samples tested for both HDPE and GPPS. The results from the DIC technique on HDPE specimens also showed unexpected behaviour in the strains mapped over the surface. Generally during a tensile test, the strains in the transverse direction will be negative, which means the material is contracting, as the specimen extends in the longitudinal direction, however, the DIC results for HDPE specimen showed some positive transverse strains in some regions. This could be as a result that some regions of the crystalline material contract as they extend, thereby creating tension in the surrounding amorphous areas as the HDPE is strained. In the GPPS specimen on the other hand the

transvers strain in were negative as the material was subjected to tensile stress which is as expected.

The strains in the longitudinal direction will be positive, which means the material is expanding, as the specimen is subjected to longitudinal stress, however, the DIC results for HDPE specimen showed some negative longitudinal strains in some regions, which indicates contraction occurring. In the GPPS specimen, the strains in the longitudinal direction were positive as expected.

The Poisson's ratio was observed to vary considerably at specimen strains below 1% and tend to settle down to a more constant value as the strain increased beyond 1%. The more constant values above 1% are in general agreement with those values reported in the literature, though there is still a small increase in 'steady' values above 1% specimen strain. The more traditional extensometer measurements will hide this result as they will average the strains and therefore give only average values for Poisson's ratio. The variations in Poisson's ratio observed go some way to explain the range of values that are reported in the literature for HDPE, though much of this will be doubtless due to varying degrees of crystallinity due to differing batch compositions and processing conditions.

In the semi-crystalline structure of the HDPE it is well established that the amorphous regions deform more than the crystalline regions within the material, and the results presented from this work are considered to be entirely consistent with the non-uniform way in which the structure is expected to deform. The work also shows that DIC can be used to reveal the more subtle nature of deformations within this type of material and helps to give a greater understanding of the structure-property relationship.

The twin microscope results showed little direct agreement with the results obtained from either the DIC technique, or those previously reported, but this was found to be primarily due to movement of the test specimen in the grips of the test machine as well as small rotations of the grips. In conclusion, the results obtained from the DIC technique for HDPE were in agreement with the results previously reported by Bhabha (2015) and also allowed a more detailed analysis of the strain development in the material. Also, there is a possibility that perhaps local relief of stresses when crazes form could lead to the modulations in lateral and longitudinal strain in the case of GPPS. Whilst in HDPE, there are localised movements of the crystal lamellae that may give the same overall observation. It is also possible that the strain range investigated would reveal deformation within the amorphous regions whilst the crystalline regions remains unaffected.

5.2 Future work

An overview of the proposed PhD work will be discussed in the order the work will be carried out in a timely manner.

Poisson's ratio (υ) was obtained and plotted using DIC technique as shown previously and the working theory is that the variation in strain and subsequently υ is a function of the crystallinity of the material. To verify the working theory is correct, the material will be mapped with the strain plot and crystallinity of regions with high strain and low strain will be determined by called Differential Scanning Calorimetry (DSC). The information acquired will be employed to clarify the behaviour in the Poisson's ratio values obtained using the DIC technique.

A structure-property relationship will be established by linking the degree of crystallinity with the mechanical properties of the material. The relations will be used in predicting the mechanical properties of the material.

Determination of the degree of crystallisation.

The degree of crystallinity of a material can be determined in numerous ways. Some methods are indirect such as density measurement and Differential Scanning Calorimetry (DSC) while X-Ray Diffraction (XRD) can give a direct measurement. The DSC method will be used to determine the crystallinity of the polymer (Ehrenstein, 2001) as small DSC samples can be cut out from the υ-mapped tensile samples. DSC is an effective analytical tool which was introduced in the 1960s used in obtaining the physical characteristics of a polymer such as; glass (T_g), crystallisation (T_c) and melting transition temperature (T_m) amongst others (Schick, 2009). DSC was selected because it is a well-established method for obtaining the degree of crystallinity in very small samples. The melting enthalpy of a fully crystallised polyethylene (286.7J/g) will be used in the calculation of the degree of crystallisation (Hitachi, 1986). The crystallisation of HDPE material differs due to the cooling time: when cooled slowly, the molecules have enough time to align and be closely packed, however when cooled rapidly the molecules are not able to align properly.

Establishing Structure-Property relationship

The DSC technique will be carried out as previously described for all samples to verify the hypothesis that the local properties will vary with the degree of crystallinity. After obtaining the crystallinity of the different regions, the results will be linked to the

mechanical properties within that region. It is anticipated that regions of high strain correlate with amorphous regions and likewise, regions with low strain correlates with crystalline regions. This relationship will help provide the ability to predict mechanical properties of polymeric materials by applying the law of mixtures.

The results used in a law of mixtures approach to determine an average Poisson's ratio and E for the material. The results should determine if a relatively simple DSC experiment on very small samples of material can be used to predict Poisson's ratio and E.

List of References

Airbus Group (2006) *Taking the lead: A350 XWB*. Available from: https://web.archive.org/web/20090327094646/http://www.eads.com/xml/content/OF00000000400004/7/19/41508197.pdf [Accessed: 1 July 2016].

Allegra, G., Corradini, P., Elias, H.-G., Geil, P. H., Keith, H. D. and Wunderlick, B. (1989) Definitions of Terms Relating to Crystalline Polymers. *Pure and Applied Chemistry*, 61(4) pp. 769–785.

Askeland, R. D. (1990) *The science and engineering of materials*. 2nd Edition, London: Chapman and Hall.

Ayoub, G., Zaïri, F., Naït-Abdelaziz, M. and Gloaguen, J. M. (2010) Modelling large deformation behaviour under loading-unloading of semicrystalline polymers: Application to a high density polyethylene. *International Journal of Plasticity*. Elsevier Ltd, 26(3) pp. 329–347.

Beijer, J. G. J. and Spoormaker, J. L. (2002) Solution strategies for FEM analysis with nonlinear viscoelastic polymers. *Computers and Structures*, 80(14–15) pp. 1213–1229.

Belgherras, M. E., Serier, B. and Zouambi, L. (2017) Elliptic crack behavior emanating from the cement mantle of the total hip prosthesis. *Polymer Testing*. Elsevier Ltd, 61, pp. 441–447.

Brown, R. (1999) *Handbook of Polymer Testing*: Physical Methods. New York: CRC Press (Plastics Engineering).

Callister, W. and David, R. (2010) *Materials Science and Engineering.* 8th Edition SI Version. John Wiley & Sons.

Cowie, J. M. G. and Arrighi, V. (2007) *Polymers: Chemistry and physics of modern materials*. 3rd Edition. CRC Press.

Ehrenstein, G. W. (2001*) Polymeric Materials: Structure, Properties, Applications*. Hanser Publishers.

Esmaeili, S., Rasouli, S., Sobouti, F. and Esmaeili, S. (2012) A moiré micro strain gauge, *Optics Communications*, 285(9) pp. 2243–2246.

Farris, S., Pozzoli, S., Biagioni, P., Duó, L., Mancinelli, S. and Piergiovanni, L. (2010) The fundamentals of flame treatment for the surface activation of polyolefin polymers – A review, *Polymer*, 51(16), pp. 3591–3605.

Frank, A., Pinter, G. and Lang, R. W. (2009) Prediction of the remaining lifetime of polyethylene pipes after up to 30 years in use*, Polymer Testing. Elsevier Ltd*, 28(7), pp. 737–745.

Hitachi. (1986). Dsc Measurement of polyethylene. Available: Hitachi-Hightech.Com/File/Global/Pdf/Products/Science/Appli/Ana/Thermal/Application_Ta_026e.Pdf. Last Accessed 10th Jan 2016.

Hoult, N. A., Andy Take, W., Lee, C. and Dutton, M. (2013) Experimental accuracy of two dimensional strain measurements using Digital Image Correlation, *Engineering Structures*, 46(0), pp. 718–726.

Hua, T., Xie, H., Wang, S., Hu, Z., Chen, P. and Zhang, Q. (2011) Evaluation of the quality of a speckle pattern in the digital image correlation method by mean subset fluctuation, *Optics & Laser Technology*, 43(1), pp. 9–13.

Jar, P.-Y. Ben (2015) Effect of tensile loading history on mechanical properties for polyethylene, *Polymer Engineering & Science*, 55(9), pp. 2002–2010.

Jerabek, M., Major, Z. and Lang, R. W. (2010) Strain determination of polymeric materials using digital image correlation, *Polymer Testing*, 29(3), pp. 407–416.

Kanokboriboon, A. (2007) An investigation on the effects of a fine-particulate filler on the properties of a rotomoulding-grade polyethylene, Society of Plastics Engineers ANTEC Conference Proceedings.

Khalajmasoumi, M., Koloor, S. S. R., Arefnia, A., Ibrahim, I. S. and Yatim, J. M. (2012) Explicit dynamic simulation of high density polyethylene beam under flexural loading condition, *Applied Mechanics and Materials*, 229-231, pp. 2150–2154.

Kiass, N., Khelif, R., Boulanouar, L. and Chaoui, K. (2005) Experimental approach to mechanical property variability through a high-density polyethylene gas pipe wall, *Journal of Applied Polymer Science,* 97(1), pp. 272–281.

Lakes, R. R. (1987) Foam structures with a negative Poisson's ratio, *American Association for the Advancement of Science*, 235(4792), pp. 1038–1040.

Lin, G., Tan, H. and Bai, X. (2014) Mechanical parameters determination of a polymeric membrane by digital image correlation, *Polymers and Polymer Composites*, 22(2), pp. 157–162.

McClung, A. J. W., Tandon, G. P., Goecke, K. E. and Baur, J. W. (2011) Non-contact technique for characterizing full-field surface deformation of shape memory polymers at elevated and room temperatures, *Polymer Testing. Elsevier Ltd*, 30(1), pp. 140–149.

Nikolov, S., Doghri, I., Pierard, O., Zealouk, L. and Goldberg, A. (2002) Multi-scale constitutive modeling of the small deformations of semi-crystalline polymers, *Journal of the Mechanics and Physics of Solids*, 50(11), pp. 2275–2302.

Peters, W. H. and Ranson, W. F. (1982) Digital Imaging Techniques In Experimental Stress Analysis, *Optical Engineering*, 21(3).

Schick, C. (2009) Differential scanning calorimetry (DSC) of semicrystalline polymers, *Analytical and Bioanalytical Chemistry*, 395(6), pp. 1589–1611.

Schreier, H., Orteu, J.-J. and Sutton, M. A. (2009) *Image correlation for shape, motion and deformation measurements: Basic concepts, theory and applications*. Boston: Springer US.

Şirin, K., Doğan, F., Çanlı, M. and Yavuz, M. (2013) Mechanical properties of polypropylene (PP) + high-density polyethylene (HDPE) binary blends: Non-isothermal degradation kinetics of PP + HDPE (80/20) Blends, *Polymers for Advanced Technologies*, 24(8), pp. 715–722.

Sutton, M., Wolters, W., Peters, W., Ranson, W. and McNeill, S. (1983) Determination of displacements using an improved digital correlation method, *Image and Vision Computing. Elsevier*, 1(3), pp. 133–139.

Tangram.co.uk. (2018). Tangram Technology Ltd. - Low temperature plastics. [online] Available at: http://www.tangram.co.uk/TI-Polymer-Low_temperature_plastics.html [Accessed 5 Aug. 2018].

Tuominen, M., Ek, M., Saloranta, P., Toivakka, M. and Kuusipalo, J. (2013) The Effect of Flame Treatment on Surface Properties and Heat Sealability of Low-Density Polyethylene Coating. *Packaging Technology and Science*, 26(4) pp. 201–214.

Tschoegl, N. W., Knauss, W. G. and Emri, I. (2002) Poisson's ratio in linear viscoelasticity - A Critical Review, *Mechanics of Time-Dependent Materials*, 6(1), pp. 3–51.

Vecchioc, K. S., Remonda, Y. and Ahzia, S. (2005) *Amorphous polymers, in Electron Microscopy of Polymers*. Berlin, Heidelberg: Springer Berlin Heidelberg.

Velosa, J. C., Nunes, J. P., Antunes, P. J., Silva, J. F. and Marques, A. T. (2008) Development of a new generation of filament wound composite pressure cylinders, *Special Issue on the 12th European Conference on Composite Materials*, ECCM 2006. Elsevier Ltd, 69(9), pp. 1348–1353.

Wang, W., Mottershead, J. E., Sebastian, C. M. and Patterson, E. A. (2011) Shape features and finite element model updating from full-field strain data*, International Journal of Solids and Structures*, 48(11–12), pp. 1644–1657.

Yan, W., Lin, R. J. T. and Bhattacharyya, D. (2006) Particulate reinforced rotationally moulded polyethylene composites - Mixing methods and mechanical properties, *Composites Science and Technology*, 66(13), pp. 2080–2088.

Appendix A

Table 5: Details of materials.

Manufacturer / Supplier.	Product	Melt flow rate	Quantity	Procure / in store
Borealis	HDPE (MG7547S pellet)	4g/10minutes	10kg	In store
	Short Glass Fibre	-	Unknown	Procure
Dow Plastics	GPPS (STYRON 637)	2.5 dg/minute	10kg	In store

Table 6: Details of machines.

Manufacturer / Supplier.	Machine	Process
Hounsfield	H10KS	Tensile testing machine
Maplin	USB microscope	Digital microscope
Dell	laptop	Computing
Thermo Electron Corporation	TSE 24 HC Prism Twin extruder machine	Compounding
Battenfeld	BA 230 CD plus	Injection moulding machine
Zwick	D-7900	Impact testing machine
Perkin Elmer	TAC 7DX	DSC
Zeiss	SUPRA^{TM} 40VP	SEM

Appendix B

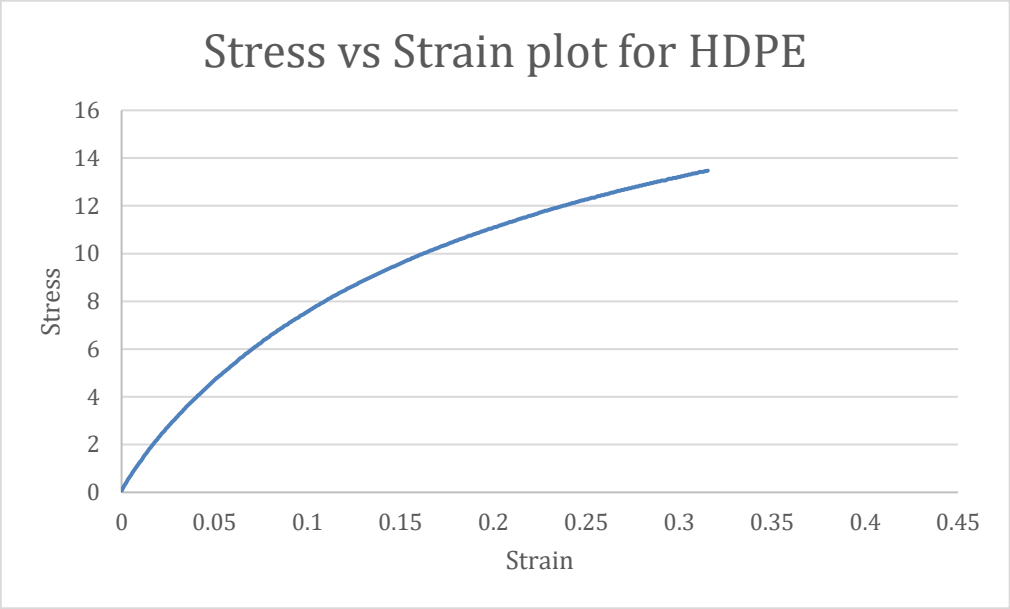

Figure 26: Stress vs strain curve indicating where images were captured for HDPE.

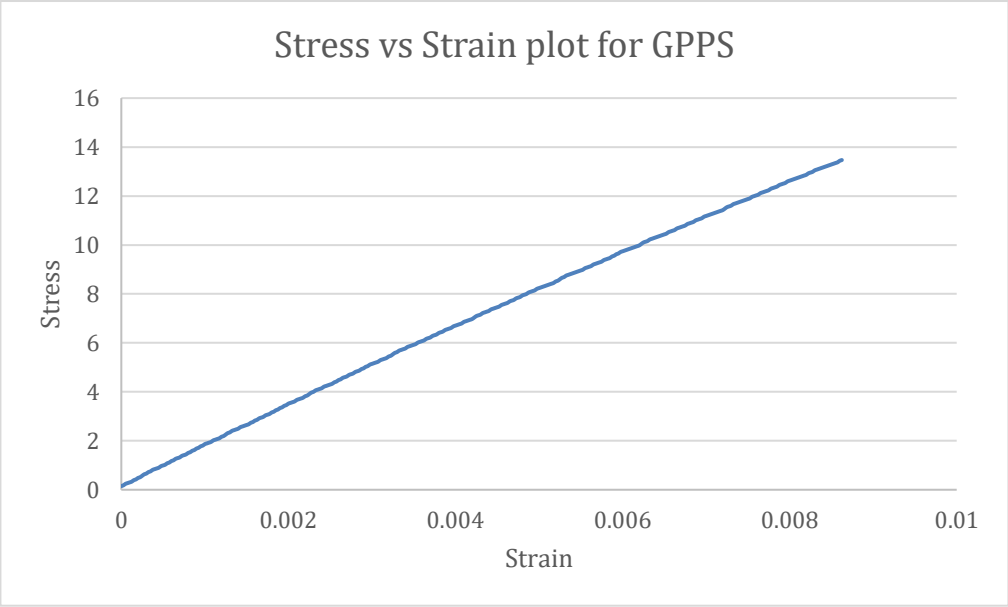

Figure 27: Stress vs strain curve indicating where images were captured for GPPS.

Appendix C

Table 7: GPPS material from tensile tests

Results for Product: TESTING GPPS MATERIAL DIC				
Batch: 1				
Curves for Specimen No:1			cross sectional area (mm^2) =	41.5744
Curve No: 1			original length (mm) =	60
Thickness =	4.06	mm		
Width =	10.24	mm		
Extension (mm)	Force (N)		Engineering stress (N/mm^2)	Engineering strain
0	6.25		0.150332897	0
0.0015	7.5		0.180399477	0.000025
0.003	10		0.240532635	0.00005
0.0045	11.25		0.270599215	0.000075
0.006	12.5		0.300665794	0.0001
0.0075	13.75		0.330732374	0.000125
0.009	16.25		0.390865533	0.00015
0.0105	17.5		0.420932112	0.000175
0.012	20		0.481065271	0.0002
0.0135	21.25		0.51113185	0.000225
0.015	23.75		0.571265009	0.00025
0.0165	26.25		0.631398168	0.000275
0.018	27.5		0.661464748	0.0003
0.0195	30		0.721597906	0.000325
0.021	31.25		0.751664486	0.00035
0.0225	33.75		0.811797645	0.000375
0.024	35		0.841864224	0.0004
0.0255	36.25		0.871930804	0.000425
0.027	37.5		0.901997383	0.00045
0.0285	40		0.962130542	0.000475
0.03	41.25		0.992197121	0.0005
0.0315	42.5		1.022263701	0.000525
0.033	45		1.08239686	0.00055
0.0345	46.25		1.112463439	0.000575
0.036	48.75		1.172596598	0.0006
0.0375	50		1.202663177	0.000625
0.039	52.5		1.262796336	0.00065
0.0405	53.75		1.292862916	0.000675
0.042	55		1.322929495	0.0007

0.0435	57.5		1.383062654	0.000725
0.045	58.75		1.413129233	0.00075
0.0465	60		1.443195813	0.000775
0.048	62.5		1.503328972	0.0008
0.0495	63.75		1.533395551	0.000825
0.051	66.25		1.59352871	0.00085
0.0525	67.5		1.623595289	0.000875
0.054	70		1.683728448	0.0009
0.0555	71.25		1.713795028	0.000925
0.057	73.75		1.773928187	0.00095
0.0585	75		1.803994766	0.000975
0.06	77.5		1.864127925	0.001
0.0615	78.75		1.894194504	0.001025
0.063	80		1.924261084	0.00105
0.0645	81.25		1.954327663	0.001075
0.066	83.75		2.014460822	0.0011
0.0675	85		2.044527401	0.001125
0.069	86.25		2.074593981	0.00115
0.0705	87.5		2.10466056	0.001175
0.072	90		2.164793719	0.0012
0.0735	91.25		2.194860299	0.001225
0.075	93.75		2.254993458	0.00125
0.0765	96.25		2.315126616	0.001275
0.078	97.5		2.345193196	0.0013
0.0795	100		2.405326355	0.001325
0.081	101.25		2.435392934	0.00135
0.0825	102.5		2.465459514	0.001375
0.084	103.75		2.495526093	0.0014
0.0855	106.25		2.555659252	0.001425
0.087	107.5		2.585725831	0.00145
0.0885	108.75		2.615792411	0.001475
0.09	110		2.64585899	0.0015
0.0915	111.25		2.67592557	0.001525
0.093	113.75		2.736058728	0.00155
0.0945	115		2.766125308	0.001575
0.096	117.5		2.826258467	0.0016
0.0975	118.75		2.856325046	0.001625
0.099	121.25		2.916458205	0.00165
0.1005	122.5		2.946524784	0.001675
0.102	123.75		2.976591364	0.0017
0.1035	126.25		3.036724523	0.001725
0.105	127.5		3.066791102	0.00175
0.1065	128.75		3.096857682	0.001775
0.108	131.25		3.156990841	0.0018

0.1095	132.5		3.18705742	0.001825
0.111	135		3.247190579	0.00185
0.1125	136.25		3.277257158	0.001875
0.114	138.75		3.337390317	0.0019
0.1155	140		3.367456897	0.001925
0.117	142.5		3.427590055	0.00195
0.1185	143.75		3.457656635	0.001975
0.12	146.25		3.517789794	0.002
0.1215	147.5		3.547856373	0.002025
0.123	148.75		3.577922953	0.00205
0.1245	150		3.607989532	0.002075
0.126	152.5		3.668122691	0.0021
0.1275	153.75		3.69818927	0.002125
0.129	155		3.72825585	0.00215
0.1305	156.25		3.758322429	0.002175
0.132	158.75		3.818455588	0.0022
0.1335	160		3.848522167	0.002225
0.135	162.5		3.908655326	0.00225
0.1365	165		3.968788485	0.002275
0.138	166.25		3.998855065	0.0023
0.1395	168.75		4.058988224	0.002325
0.141	170		4.089054803	0.00235
0.1425	171.25		4.119121382	0.002375
0.144	172.5		4.149187962	0.0024
0.1455	175		4.209321121	0.002425
0.147	176.25		4.2393877	0.00245
0.1485	177.5		4.26945428	0.002475
0.15	178.75		4.299520859	0.0025
0.1515	180		4.329587438	0.002525
0.153	182.5		4.389720597	0.00255
0.1545	183.75		4.419787177	0.002575
0.156	186.25		4.479920336	0.0026
0.1575	187.5		4.509986915	0.002625
0.159	190		4.570120074	0.00265
0.1605	191.25		4.600186653	0.002675
0.162	192.5		4.630253233	0.0027
0.1635	195		4.690386392	0.002725
0.165	196.25		4.720452971	0.00275
0.1665	197.5		4.75051955	0.002775
0.168	200		4.810652709	0.0028
0.1695	201.25		4.840719289	0.002825
0.171	202.5		4.870785868	0.00285
0.1725	205		4.930919027	0.002875
0.174	206.25		4.960985607	0.0029

0.1755	208.75		5.021118765	0.002925
0.177	210		5.051185345	0.00295
0.1785	212.5		5.111318504	0.002975
0.18	213.75		5.141385083	0.003
0.1815	215		5.171451663	0.003025
0.183	216.25		5.201518242	0.00305
0.1845	217.5		5.231584821	0.003075
0.186	220		5.29171798	0.0031
0.1875	221.25		5.32178456	0.003125
0.189	222.5		5.351851139	0.00315
0.1905	223.75		5.381917719	0.003175
0.192	226.25		5.442050877	0.0032
0.1935	227.5		5.472117457	0.003225
0.195	230		5.532250616	0.00325
0.1965	232.5		5.592383775	0.003275
0.198	233.75		5.622450354	0.0033
0.1995	236.25		5.682583513	0.003325
0.201	237.5		5.712650092	0.00335
0.2025	238.75		5.742716672	0.003375
0.204	240		5.772783251	0.0034
0.2055	242.5		5.83291641	0.003425
0.207	243.75		5.86298299	0.00345
0.2085	245		5.893049569	0.003475
0.21	246.25		5.923116148	0.0035
0.2115	247.5		5.953182728	0.003525
0.213	250		6.013315887	0.00355
0.2145	251.25		6.043382466	0.003575
0.216	252.5		6.073449046	0.0036
0.2175	253.75		6.103515625	0.003625
0.219	256.25		6.163648784	0.00365
0.2205	257.5		6.193715363	0.003675
0.222	258.75		6.223781943	0.0037
0.2235	261.25		6.283915102	0.003725
0.225	262.5		6.313981681	0.00375
0.2265	263.75		6.34404826	0.003775
0.228	266.25		6.404181419	0.0038
0.2295	267.5		6.434247999	0.003825
0.231	268.75		6.464314578	0.00385
0.2325	271.25		6.524447737	0.003875
0.234	272.5		6.554514317	0.0039
0.2355	273.75		6.584580896	0.003925
0.237	275		6.614647475	0.00395
0.2385	277.5		6.674780634	0.003975
0.24	278.75		6.704847214	0.004

0.2415	280		6.734913793	0.004025
0.243	281.25		6.764980373	0.00405
0.2445	282.5		6.795046952	0.004075
0.246	285		6.855180111	0.0041
0.2475	286.25		6.88524669	0.004125
0.249	287.5		6.91531327	0.00415
0.2505	288.75		6.945379849	0.004175
0.252	290		6.975446429	0.0042
0.2535	292.5		7.035579587	0.004225
0.255	295		7.095712746	0.00425
0.2565	296.25		7.125779326	0.004275
0.258	297.5		7.155845905	0.0043
0.2595	300		7.215979064	0.004325
0.261	301.25		7.246045643	0.00435
0.2625	302.5		7.276112223	0.004375
0.264	303.75		7.306178802	0.0044
0.2655	306.25		7.366311961	0.004425
0.267	307.5		7.396378541	0.00445
0.2685	308.75		7.42644512	0.004475
0.27	310		7.4565117	0.0045
0.2715	311.25		7.486578279	0.004525
0.273	313.75		7.546711438	0.00455
0.2745	315		7.576778017	0.004575
0.276	316.25		7.606844597	0.0046
0.2775	317.5		7.636911176	0.004625
0.279	320		7.697044335	0.00465
0.2805	321.25		7.727110914	0.004675
0.282	322.5		7.757177494	0.0047
0.2835	325		7.817310653	0.004725
0.285	326.25		7.847377232	0.00475
0.2865	327.5		7.877443812	0.004775
0.288	330		7.93757697	0.0048
0.2895	331.25		7.96764355	0.004825
0.291	332.5		7.997710129	0.00485
0.2925	335		8.057843288	0.004875
0.294	336.25		8.087909868	0.0049
0.2955	337.5		8.117976447	0.004925
0.297	338.75		8.148043026	0.00495
0.2985	341.25		8.208176185	0.004975
0.3	342.5		8.238242765	0.005
0.3015	343.75		8.268309344	0.005025
0.303	345		8.298375924	0.00505
0.3045	346.25		8.328442503	0.005075
0.306	347.5		8.358509083	0.0051

0.3075	348.75		8.388575662	0.005125
0.309	350		8.418642241	0.00515
0.3105	351.25		8.448708821	0.005175
0.312	353.75		8.50884198	0.0052
0.3135	355		8.538908559	0.005225
0.315	357.5		8.599041718	0.00525
0.3165	360		8.659174877	0.005275
0.318	361.25		8.689241456	0.0053
0.3195	363.75		8.749374615	0.005325
0.321	365		8.779441195	0.00535
0.3225	366.25		8.809507774	0.005375
0.324	367.5		8.839574353	0.0054
0.3255	368.75		8.869640933	0.005425
0.327	370		8.899707512	0.00545
0.3285	371.25		8.929774092	0.005475
0.33	372.5		8.959840671	0.0055
0.3315	373.75		8.989907251	0.005525
0.333	376.25		9.050040409	0.00555
0.3345	377.5		9.080106989	0.005575
0.336	378.75		9.110173568	0.0056
0.3375	380		9.140240148	0.005625
0.339	382.5		9.200373307	0.00565
0.3405	383.75		9.230439886	0.005675
0.342	385		9.260506466	0.0057
0.3435	386.25		9.290573045	0.005725
0.345	387.5		9.320639624	0.00575
0.3465	390		9.380772783	0.005775
0.348	391.25		9.410839363	0.0058
0.3495	392.5		9.440905942	0.005825
0.351	393.75		9.470972522	0.00585
0.3525	396.25		9.53110568	0.005875
0.354	397.5		9.56117226	0.0059
0.3555	400		9.621305419	0.005925
0.357	401.25		9.651371998	0.00595
0.3585	403.75		9.711505157	0.005975
0.36	405		9.741571736	0.006
0.3615	406.25		9.771638316	0.006025
0.363	407.5		9.801704895	0.00605
0.3645	408.75		9.831771475	0.006075
0.366	410		9.861838054	0.0061
0.3675	411.25		9.891904634	0.006125
0.369	412.5		9.921971213	0.00615
0.3705	413.75		9.952037792	0.006175
0.372	415		9.982104372	0.0062

0.3735	417.5		10.04223753	0.006225
0.375	420		10.10237069	0.00625
0.3765	421.25		10.13243727	0.006275
0.378	422.5		10.16250385	0.0063
0.3795	425		10.22263701	0.006325
0.381	426.25		10.25270359	0.00635
0.3825	427.5		10.28277017	0.006375
0.384	428.75		10.31283675	0.0064
0.3855	430		10.34290333	0.006425
0.387	431.25		10.3729699	0.00645
0.3885	432.5		10.40303648	0.006475
0.39	433.75		10.43310306	0.0065
0.3915	435		10.46316964	0.006525
0.393	437.5		10.5233028	0.00655
0.3945	438.75		10.55336938	0.006575
0.396	440		10.58343596	0.0066
0.3975	441.25		10.61350254	0.006625
0.399	443.75		10.6736357	0.00665
0.4005	445		10.70370228	0.006675
0.402	446.25		10.73376886	0.0067
0.4035	447.5		10.76383544	0.006725
0.405	448.75		10.79390202	0.00675
0.4065	451.25		10.85403518	0.006775
0.408	452.5		10.88410175	0.0068
0.4095	453.75		10.91416833	0.006825
0.411	455		10.94423491	0.00685
0.4125	457.5		11.00436807	0.006875
0.414	458.75		11.03443465	0.0069
0.4155	460		11.06450123	0.006925
0.417	461.25		11.09456781	0.00695
0.4185	463.75		11.15470097	0.006975
0.42	465		11.18476755	0.007
0.4215	466.25		11.21483413	0.007025
0.423	467.5		11.24490071	0.00705
0.4245	468.75		11.27496729	0.007075
0.426	470		11.30503387	0.0071
0.4275	471.25		11.33510045	0.007125
0.429	472.5		11.36516703	0.00715
0.4305	473.75		11.39523361	0.007175
0.432	475		11.42530018	0.0072
0.4335	477.5		11.48543334	0.007225
0.435	480		11.5455665	0.00725
0.4365	481.25		11.57563308	0.007275
0.438	482.5		11.60569966	0.0073

0.4395	485		11.66583282	0.007325
0.441	486.25		11.6958994	0.00735
0.4425	487.5		11.72596598	0.007375
0.444	488.75		11.75603256	0.0074
0.4455	490		11.78609914	0.007425
0.447	491.25		11.81616572	0.00745
0.4485	492.5		11.8462323	0.007475
0.45	493.75		11.87629888	0.0075
0.4515	495		11.90636546	0.007525
0.453	497.5		11.96649861	0.00755
0.4545	498.75		11.99656519	0.007575
0.456	500		12.02663177	0.0076
0.4575	501.25		12.05669835	0.007625
0.459	503.75		12.11683151	0.00765
0.4605	505		12.14689809	0.007675
0.462	506.25		12.17696467	0.0077
0.4635	507.5		12.20703125	0.007725
0.465	508.75		12.23709783	0.00775
0.4665	511.25		12.29723099	0.007775
0.468	512.5		12.32729757	0.0078
0.4695	513.75		12.35736415	0.007825
0.471	515		12.38743073	0.00785
0.4725	517.5		12.44756389	0.007875
0.474	518.75		12.47763046	0.0079
0.4755	520		12.50769704	0.007925
0.477	521.25		12.53776362	0.00795
0.4785	523.75		12.59789678	0.007975
0.48	525		12.62796336	0.008
0.4815	526.25		12.65802994	0.008025
0.483	527.5		12.68809652	0.00805
0.4845	528.75		12.7181631	0.008075
0.486	530		12.74822968	0.0081
0.4875	531.25		12.77829626	0.008125
0.489	532.5		12.80836284	0.00815
0.4905	533.75		12.83842942	0.008175
0.492	535		12.868496	0.0082
0.4935	537.5		12.92862916	0.008225
0.495	538.75		12.95869574	0.00825
0.4965	540		12.98876232	0.008275
0.498	542.5		13.04889547	0.0083
0.4995	543.75		13.07896205	0.008325
0.501	545		13.10902863	0.00835
0.5025	546.25		13.13909521	0.008375
0.504	547.5		13.16916179	0.0084

0.5055	548.75		13.19922837	0.008425
0.507	550		13.22929495	0.00845
0.5085	551.25		13.25936153	0.008475
0.51	552.5		13.28942811	0.0085
0.5115	553.75		13.31949469	0.008525
0.513	555		13.34956127	0.00855
0.5145	556.25		13.37962785	0.008575
0.516	558.75		13.43976101	0.0086
0.5175	560		13.46982759	0.008625

Appendix D

Properties and Modelling of Rotational Moulding Materials

Eromosele Odigie Akhigbe

Manchester Metropolitan University

School of Engineering, Manchester Metropolitan University, Manchester M1 5GD

eromosele.akhigbe@stu.mmu.ac.uk

Introduction

Rotational moulding (Roto-moulding) is a widely used process of producing large hollow plastic products like kayaks, storage tanks and so on. The static uniaxial tension test is probably the simplest and most widely used mechanical test. This uniaxial tensile test is used to determine most of the material properties such as young modulus, Poisson ratio, tensile strength and so on. Different video-based techniques have been used in many of the reported attempts to measure the true stress–strain relation of polymers. The use of image processing technique has gained more recognition in recent years due to the advantages over using strain gauge.
The purpose of investigating the material properties is to provide reliable data for finite element simulation and to compare with previous research on Poisson's ratio values for polymeric materials. Poisson ratio for the particular High-density polyethylene (HDPE) because it typically varies between 0 to 0.5.
As more complex performance structures are being designed and manufactured with polymers, the need arises to investigate both mechanical properties and material behaviour so as to determine their structural response.

Methodology

In order to avoid both contact and sensitivity issues, non-contact method using high resolution microscopes along with image processing software was applied to characterise material properties.
The use of novel twin microscope technique to track markers at appropriate spacing, one on either side of the of HDPE test specimen while simultaneously subjected to tensile test. The images derived from the twin microscope are then processed using image processing techniques to determine the stain.

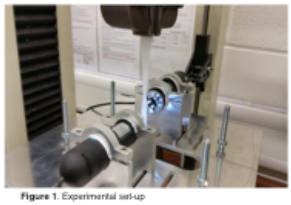

Figure 1. Experimental set-up

Experimental setup
Due to the sensitivity of the experiment, it was needful to design a platform on which the microscope will be firmly positioned. The rig is also used to elevate the microscope to the desired height. To ensure that the microscope is horizontally leveled, a plum was used to balance the Platform.

Preparation of Test Piece
Markers were placed on both sides of a HDPE specimen with a height gauge and black ink was applied to indicate the point for high contrast ratio.

Calibrating ImageJ
The specimen was clamped into the jaws of a tensometer and each microscope was adjusted to obtain a clear and vivid image of the marker. Without adjusting the settings for the microscope, the specimen was replaced by a Vernier calliper. An image of the calliper was captured with both microscopes with the jaws set to a known fixed length and imported into ImageJ. On the image of the Vernier calliper, a line was drawn on the length of the jaws and the known distance and unit was entered in order to set a global scale. After the calibration was done, the images of the test piece were imported into ImageJ so as to measure the displacement of the markers.

Results

A typical force vs extension curve was obtained after carrying out the tensile test.
Poisson's ratio (v) was calculated from the ratio of transverse and axial strains from the images obtained at intervals of 50N and test speed of 0.5mm/min while the material was still with the elastic limit.
The initial results from the twin microscope technique shows an oscillating pattern in the Poisson's ratio and not just as a constant figure.

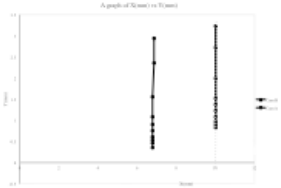

Figure 2: A plot of the tracked marker placed on the sample.

Figure 3: A plot of the oscillating value of Poisson's ratio derived from the sample.

Further work

Using the digital image correlation (DIC) approach to investigate strain in the sample and then compare the results with that obtained from novel twin microscope method and observe if it correlates…

Conclusions

The research shows that the value of the Poisson's ratio recorded from the twin microscope method is not constant, in order to achieve a more realistic results from Finite Element Analysis mostly in very sensitive and complex models, it is recommended that properties of the material be obtained through a valid process.

References

Kanoktzoglou, A. (2007) *An investigation on the effects of a Fine-particulate filler on the properties of a rotomoulding-grade polyethylene.*

Disco, L. G., Crawford, R., Kearns, M. and Geiger, N. (2006) 'Rotational molding of plastics: Comparison of simulation and experimental results for an axisymmetric mold.' *Polymer Engineering & Science*, 46(8) pp. 1158-1164.

Crawford, R. J. and Throne, J. L. *Rotational Molding Technology*. William Andrew Publishing/Plastics Design Library.

Brown, R. P. (1999) *Handbook of Polymer Testing: Physical Methods*. Marcel Dekker Incorporated.

Khalajmasoumi, M., Kolour, S. S. R., Arefnia, A., Ibrahim, I. S. and Yelim, J. M. (2012) *Explicit dynamic simulation of high density polyethylene beam under flexural loading condition*. Kuala Lumpur. 2150-2154-page handout, distributed in lecture 229-231 for module

Dowling, N. E. (1993) *Mechanical Behaviour of Materials*. 3rd edition. Pearson Education Inc.

Figure 28: Poster presentation at the faculty SciEng Conference 2015.

Appendix E

Gantt chart

The project is broken down into stages with duration.